Conversion of inlet temperature distortions to vorticity for an axial-flow compressor.

Iverson, Michael Martin

Monterey, California. Naval Postgraduate School

THESIS

Conversion of Inlet Temperature Distortions to Vorticity for an Axial-Flow Compressor

by

Michael Martin Iverson

Thesis Advisor: A. E. Fuhs

June 1972

NAVAL POSTGRADUATE SCHOOL
Monterey, California

THESIS

Conversion of Inlet Temperature Distortions to Vorticity for an Axial-Flow Compressor

by

Michael Martin Iverson

Thesis Advisor: A. E. Fuhs

June 1972

Conversion of Inlet Temperature Distortions to Vorticity for an Axial-Flow Compressor

by

Michael Martin Iverson
Lieutenant Commander, United States Navy
B.S., California State Polytechnic College, 1963

Submitted in partial fulfillment of the
requirements for the degree of

MASTER OF SCIENCE IN AERONAUTICAL ENGINEERING

from the
NAVAL POSTGRADUATE SCHOOL
June 1972

Author [redacted]

Approved by: [redacted]
Thesis Advisor

[redacted]
Chairman, Department of Aeronautics

[redacted]
Academic Dean

ABSTRACT

A survey of the literature on pressure, temperature and foreign gas inlet distortions is made. For interpretation of the influence of inlet distortion on engine stability, a break is made with distortion methods which use temperature or pressure distortion maps. The distortion in the form of temperature contours is transformed to vorticity using appropriate equations derived for both incompressible and compressible flow. Crocco's theorem has been expanded in scope to include multispecie, nonuniform, perfect gas mixtures. The derivation of the equations and specialization to cases of interest involved a thorough order of magnitude analysis. A numerical solution of Poisson's equation as formulated by Squire and Winter to describe secondary flow arising from convected vorticity is presented. Deficient areas of knowledge relating to the general temperature/foreign gas problem are outlined. A conceptual model involving compressor stage transfer functions and feedback mechanisms is introduced and discussed at several points. Although not essential to understanding the vorticity-stall logic chain, this model is a useful conceptual tool and may be worthy of additional study.

TABLE OF CONTENTS

LIST OF TABLES

LIST OF FIGURES

SYMBOLS[1]

C_p	specific heat for a mixture of perfect gases
c_p	specific heat for a single perfect gas
D	matrix of finite difference coefficients
FG	foreign gas - variations of γ and R
G	forward transfer function
H	feedback transfer function
h	specific enthalpy
M	Mach number
m	mass/unit volume
n	normal direction in natural coordinates
P	pressure
q	scalar velocity
r	radial displacement in cylindrical coordinates
R_o	universal gas constant
R	$R_o/\bar{m}$
s	specific entropy
T	temperature
TFG	temperature and foreign gas - variations in T, γ and R
U	velocity
v	velocity perturbation
w	velocity perturbation
y	coordinate direction perpendicular to cascade span

---

[1]There is a variation of this notation in Appendices A,B,E, and G. Where such occurs, it is clearly indicated.

z axial displacement in cylindrical coordinates

Γ circulation

γ ratio of specific heats

Δ finite difference

ε flow turning angle Eq. (19), order of magnitude

θ circumferential displacement in cylindrical coordinates

ξ streamwise vorticity

ρ density

ϕ angle between principal normal and the normal to the Bernoulli surface

ψ stream function

Ω total flow vorticity

ω component of flow vorticity

Subscript

r radial component

t stagnation quantity

z axial (streamwise) component

θ circumferential component

1 inlet

2 outlet

Superscript

$-$ mean value

$'$ dimensionless quantity

ACKNOWLEDGEMENT

The author gratefully acknowledges his indebtedness to Professor Allen E. Fuhs for his initiation of the topic and for his assistance during the research. The encouragement and freedom of direction given the author is sincerely appreciated.

The author also acknowledges the encouragement and perseverance of his wife, Nancy, whose understanding made this effort possible.

I. INTRODUCTION

Turbojet stability is often defined in an inverse sense - in terms of instability. More specifically the turbojet stability is defined by the components most susceptible to instabilities - fans and compressors [Ref.1]. For a compressor characteristic (pressure-ratio versus corrected flow at constant speed) the border between stable and unstable operation is the point of maximum pressure ratio. At this point the blade loading is such that the blades are aerodynamically stalled. The resulting unsteady phenomenon is called surge. The difference between the pressure-ratio at the point of surge and the pressure-ratio at which the compressor is operating is defined as stability margin.

A common factor causing compressor surge is non-uniform inlet flow. The non-uniformities at the inlet are popularly termed inlet distortions.

The stability margin of current high specific energy gas turbine engines is at what might be termed a practical, if not critical, minimum. A result is that engine inlet distortions can readily produce instability in the fan and/or compressor. For certification purposes, the instability problem can be avoided by increasing stall margin which generally is at the expense of engine performance. The most prevalent inlet distortions causing instability are total pressure and total temperature. These can be

further categorized [Ref. 1] as:

Inlet Pressure Spatial Distortion

Inlet Pressure Fluctuations

Inlet Pressure Ramps

Inlet Temperature Spatial Distortion

Inlet Temperature Ramps

Pressure distortions are seemingly the most common in occurrence and thus have been the object of widest study. References 2-14 provide insight and additional literature sources for further review of this problem.

Temperature distortions in turbojets received some early investigation [Refs. 15, 16, and 17] which centered on the transient category. More recently Rudey and Antl [Ref. 18] investigated both spatial and transient temperature effects on a turbofan engine compressor system.

Other recent investigations have concentrated on the inherently related areas of steam and armament exhaust ingestion. Tomassetti [Ref. 19] performed extensive work on the TF30 turbofan engine. He concluded that the primary factors causing instability were:

Inlet Temperature Distortion

Non-homogeneity of Inlet Gas Properties

Ingestion of Liquid Condensate

Tomassetti developed a steam Enviromental Factor as means of comparing results. Reference 20 modified the Environmental Factor to accommodate additional variables. Also investigating the TF30 steam problem were Mallett and

Parcells [Ref. 21] and Worobei [Ref. 22]. They reached conclusions similar to Rudey and Antl. Additionally, Mallett and Parcells noted a dependency of stability margin on the individual compressor design.

Armament gas ingestion has been the subject of several studies at the Naval Air Propulsion Test Center (NAPTC). Rich and Reale [Ref. 23] investigated the effects of sea level missile exhaust gas ingestion on the J52-P-6A engine. The missile exhaust gas simulator used in NAPTC testing is described by Rich [Ref. 24]. Reference 25 publishes the results of rocket gas ingestion by the TF34 engine, which is used on the S-3 Viking and A-10A attack aircraft.

To gain further insight into the temperature problem, this paper will develop a mathematical model to describe the inlet distortion in terms of vorticity. This is a new approach in contrast to the classical approach of a total temperature map. It is an aid to a better examination of the flow mechanisms involved with inlet temperature distortions.

II. TEMPERATURE DISTORTION

A. TEMPERATURE SOURCES

Engine instability due to temperature or foreign gas distortion has not been widely studied relative to distortion from variation in stagnation pressure. Perhaps the reason is the complexity of the investigation due to the type of temperature distortion sources: i.e. catapult steam, Fig. 1; rocket or missile armament exhaust gas, Fig. 2; spent gun propellants; exhaust of other aircraft; and uneven temperature due to heating of air above runways and taxiways. The steam ingestion problem is of importance to carrier launched aircraft, especially those with low-mounted inlets on the aircraft centerline, i.e. A-7. The ingestion of armament gas is mainly encountered by tactical aircraft. In addition to the detrimental effects of engine stall caused by the swallowing of rocket plumes, explosions may occur in the engine (the exhausts of rocket plumes are usually fuel rich). In formation flying or during aerial refueling an aircraft may be subjected to the exhaust gases of the leading aircraft. Uneven heating of air can occur at airports; air above runways, particularly blacktop runways, can be considerably hotter than the ambient air. During taxi or takeoff the aircraft engine can swallow streamtubes of air with this uneven temperature distribution. It has been found that some aircraft with ejector nozzles

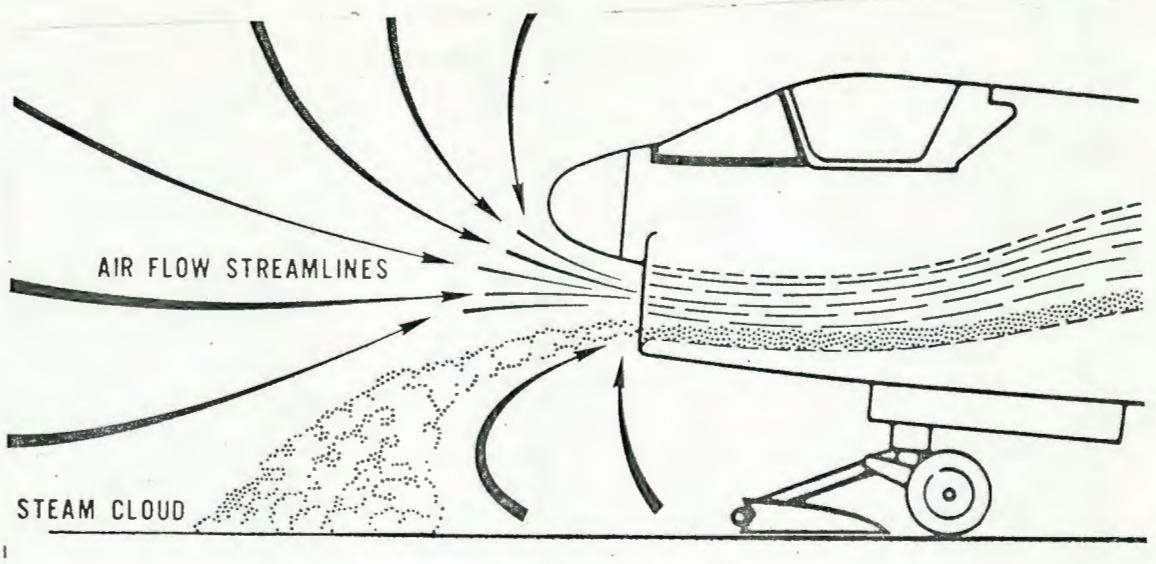

Figure 1. Catapult Steam Ingestion

(adapted from Ref. 21)

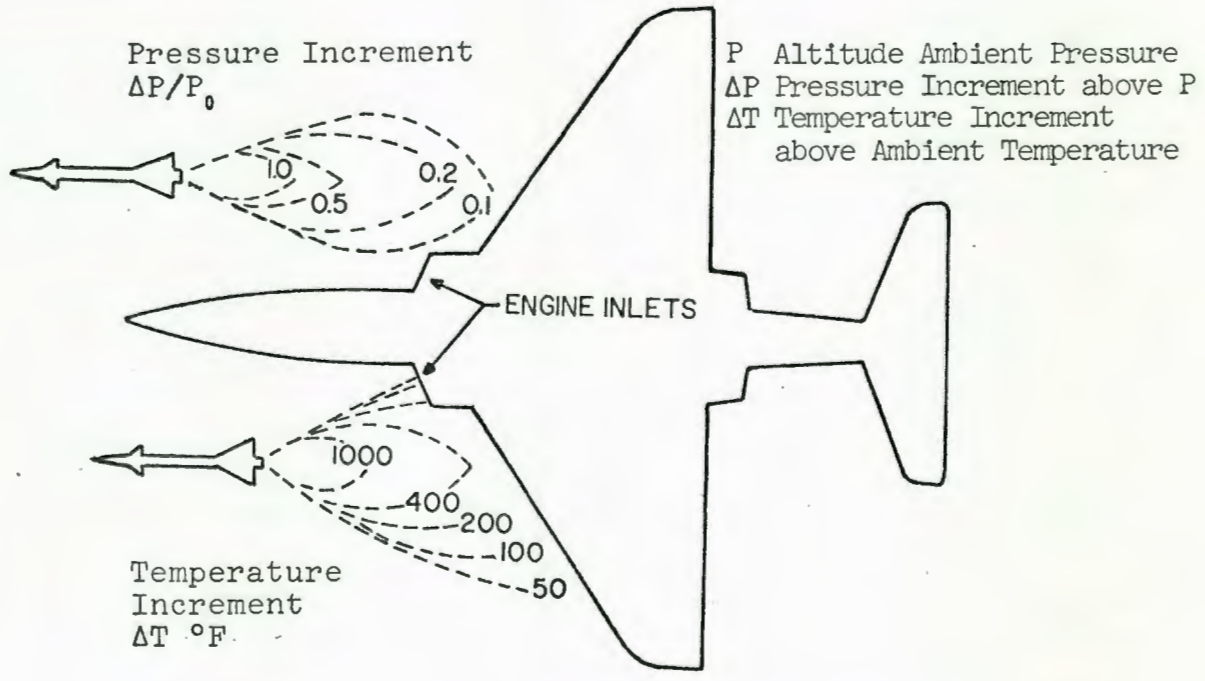

Figure 2. Missile Exhaust Gas Ingestion

(adapted from Ref. 24)

may experience temperature-induced stall while taxiing downwind. Wind blowing up the tailpipe carries air along the secondary air passages where it is heated by hot engine components and thence into the compressor.

Granted, sources of temperature distortion appear in limited situations. This does not mean the problem is insignificant. Certainly, an engine stall during an aircraft carrier catapult launch is critical. Likewise engine instability during air-to-air or air-to-ground combat maneuvers for aircraft is serious.

B. CHARACTERISTICS OF TEMPERATURE SOURCES

From the discussion of possible temperature distortion sources in the previous section, there are three characteristics that should be noted: 1. The distortion source is independent of the affected inlet-engine system. 2. The distortions may be both spatial and/or transient. and 3. Foreign gases may also be a distortion source. A brief discussion of each of these characteristics is warranted.

Necessarily, some definitions are required prior to the discussion. When the word "temperature" is used, it refers to total temperature. If static temperature is being discussed, it will be clearly indicated as such. The phrases "temperature and foreign gas" and "foreign gas" will be used with sufficient frequency to warrant the abbreviation TFG and FG respectively. A symbols sheet on page 8 provides a complete listing of definitions.

The significance of the independence of the source lies in the possibility of eliminating the distortion instabilities by removal of the source. A major part of the effort in solving the A-7 steam ingestion problem involved minimizing the source of steam [Refs. 19 and 22]. The aircraft exhaust problem can be minimized by judicious pilot techniques. Conversely, the removal of the source of armament gas is unlikely to provide a satisfactory solution. In examining the TFG problem, independence of source and engine should be kept in mind as a potentially controllable variable.

When examined from the P_t or T_t map viewpoint, spatial distortions can be divided into circumferential and radial distortions, as illustrated in Figs. 3a and 3b. In the fan engine, the circumferential distortion causes a shift in the surge line of the fan and compressor [Ref. 1]. Figure 4 is representative of this shift. Radial distortion can have similar effects except that the fan can cause attenuation of the distortion leaving the fan resulting in a lesser

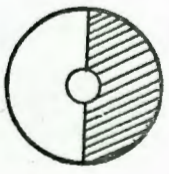

Circumferential Distortion

(a)

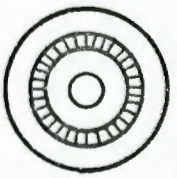

Radial Distortion

(b)

Figure 3. Spatial Distortions

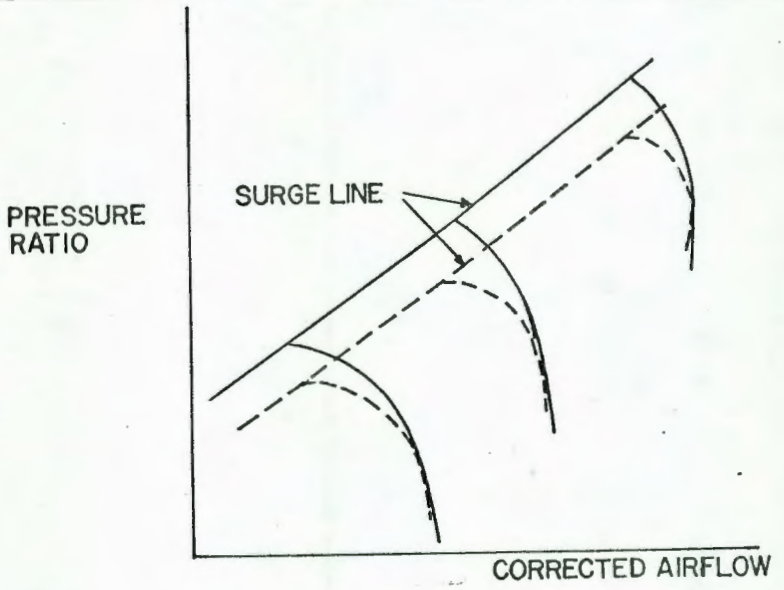

Figure 4. Effect of Spatial Distortion

(adapted from Ref. 1)

distortion level [Ref. 1]. In practice the distortions are composed of elements of both [Ref. 1].

Transient or ramp temperature distortions may result in compressor response as shown in Fig. 5. Analysis of this problem involves unsteady aerodynamics and is discussed in a later section of this thesis.

The effect of the presence of FG is mainly in changing the thermal and caloric properties of the mixture.[1] These gas properties, ratio of specific heats (γ) and gas constant ($R_o/\bar{m}$) then become variables of interest. Any model of TFG distortion (e.g. due to steam or rocket exhaust) must account for changes of these properties. The instance of no FG (e.g. hot runway) then becomes a special case.

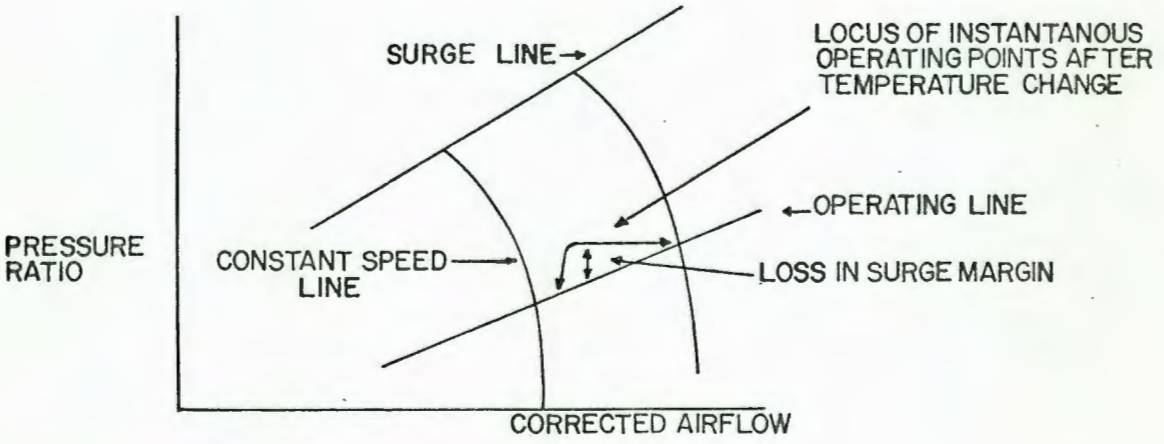

Figure 5. Effect of Temperature Ramp

(adapted from Ref. 1)

---

[1]Additional effects in the form of diffusion, condensation and chemical reactions can be present. These phenomena will not be considered by this thesis.

III. INLET DISTORTION AND VORTICITY

The efforts to solve the distortion-induced instability problem have in the past been studied independently by one of two design groups - inlet or blade-cascade. The inlet group concentrates on analysis of instabilities utilizing events occurring at the compressor face i.e. inlet distortion. Their interpretation must be based on the distortion's influence on compressor internal aerodynamics. The blade-cascade group analyzes blade and cascade response to various flow situations. In terms of solutions to current distortion-instability problems, the inlet group efforts are vital. In achieving the ultimate goal of accurate prediction of flow of an arbitrary compressor with arbitrary inlet flow, it seems the blade-cascade group efforts offer most promise. A germane question is "Can the efforts of both groups be interfaced?"

The approach of the inlet group to analyzing compressor inlet distortions involves the use of a compressor map (a series of maps for time-dependent situations) of inlet isotherms or isobars. An inlet map of the second stage would show the inlet distortion as modified by the aerodynamic influence of the first stage. Mokelke [Ref. 26] found through

experiment that the inlet guide vanes had very little effect on distortion whereas noticeable alteration was present after the first stage. The term aerodynamic influence encompasses the phenomena of shed vortices due to non-uniform and/or unsteady lift and cascade secondary flows. This aerodynamic influence is precisely the object of study of the blade-cascade group. It actually can be viewed as a transfer function. If one knew or could predict the transfer function of each stage, a large step would have been taken toward the previously mentioned goal. To begin the transfer function process, inlet distortion maps, temperature and/or pressure, must be converted into the conceptually compatible aerodynamic influence quantities.

Imagine a compressor stage preceding the first stage of an actual compressor. For identification call it the zeroth stage. The function of this imaginary stage is to transform an initially uniform flow into a flow with aerodynamic distortion patterns identical to the actual TFG (or pressure) distortion pattern. In essence the first stage of the compressor is affected by the aerodynamic influence of the zeroth stage. Thus the zeroth stage offers a way to view inlet distortion in the same physical sense it affects the first stage. It is also grounds for considering an interface between the inlet and blade-cascade group. The fluid mechanism involved is vorticity.

The logic chain into which vorticity fits involves:

1. conversion of distortion maps into vorticity maps;

2. evaluation of vorticity maps to determine changes in compressor blade loading; 3. utilization of blade loading to evaluate stall criteria; and 4. decision as to whether stall will or will not occur. The notions of aerodynamic transfer function and zeroth stage are not essential in understanding the logic chain. They are introduced as convenient ways of visualizing distortions in terms of vorticity. In fact, the zeroth stage is analogous to Marble's actuator disk model [Refs. 27 and 28] which describes the flow through a single blade row.

Before developing the vorticity relationships, a discussion of the elements of aerodynamic influence is considered necessary. The concept of circulation about a wing is well-known. If the lift changes, the circulation changes, resulting in shed vortices. The unsteady and cascade secondary flow effects are considerably more complex.

A. BLADE AND CASCADE UNSTEADY FLOW

Even if the flow entering the first stage is steady, it is not difficult to imagine a circumferential distortion causing unsteady flow over a rotor blade. In fact, Carta [Ref. 29] found that if the blade-passing reduced frequency was greater than 0.1, the flow is considered to be unsteady. During steady operation of a compressor the interference effects of the cascades are unsteady [Ref. 30].

Samoylovich [Ref. 31] has divided the unsteady phenomena into two groups: 1. purely aerodynamic unsteady phenomena; and 2. phenomena requiring coupling between the aerodynamic

and mechanical characteristics (aeroelastic effects). To limit the scope of this discussion, the assumption of infinitely rigid blades is made.[1]

It has been shown by Carta [Ref. 29] that unsteady flow over an airfoil delays stall which produces unsteady lift coefficients above those of steady flow (Figs. 6a and 6b). He also found that the rate of change of incidence angle had a major effect on the unsteady response (i.e. note the severity of $dC_N/d\alpha$ in Fig. 6a). The overshoot of C_N is due to the large reduction of adverse pressure gradient [Ref.7]. Ericsson and Redding [Ref. 32] explained the overshoot and undershoot as being caused by: 1. the effect of induced flow acceleration on the adverse pressure gradient; and 2. the effect of the induced change of effective Reynolds number or turbulence level on the boundary layer.

From basic airfoil theory, changes in lift require changes in wing circulation. Therefore unsteady lift produces an unsteady vortex wake. These vortices influence the flow about the originating airfoil. Additionally, they are swept downstream where they contribute to the interference effects. The interference effects are not necessarily detrimental. Shorr and Reddy [Ref. 33] found that in comparison with a single airfoil the amplitude of the unsteady lift coefficient for cascades reduces more slowly with increasing frequency.

---

[1]For a comprehensive treatment of aeroelastic vibration in turbomachine cascades, see Samoylovich [Ref. 31].

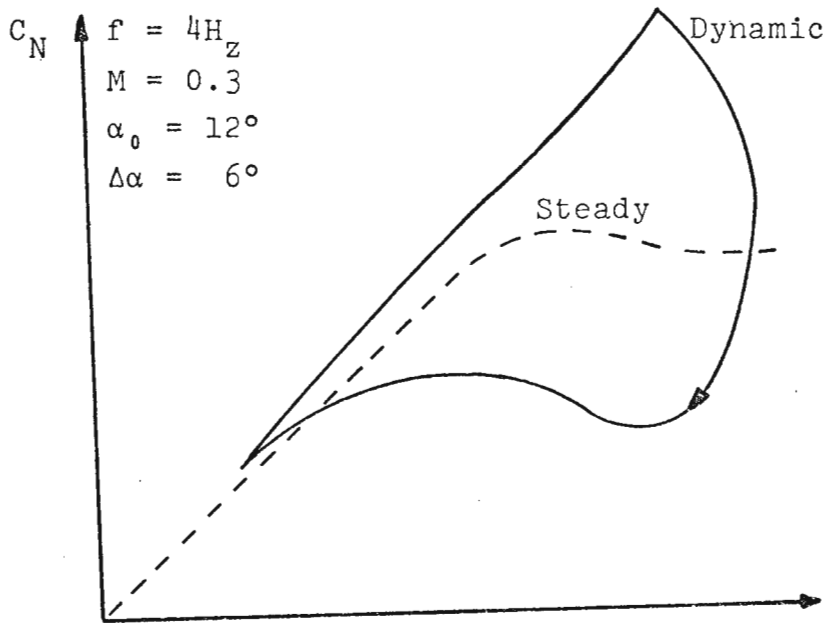

(a)

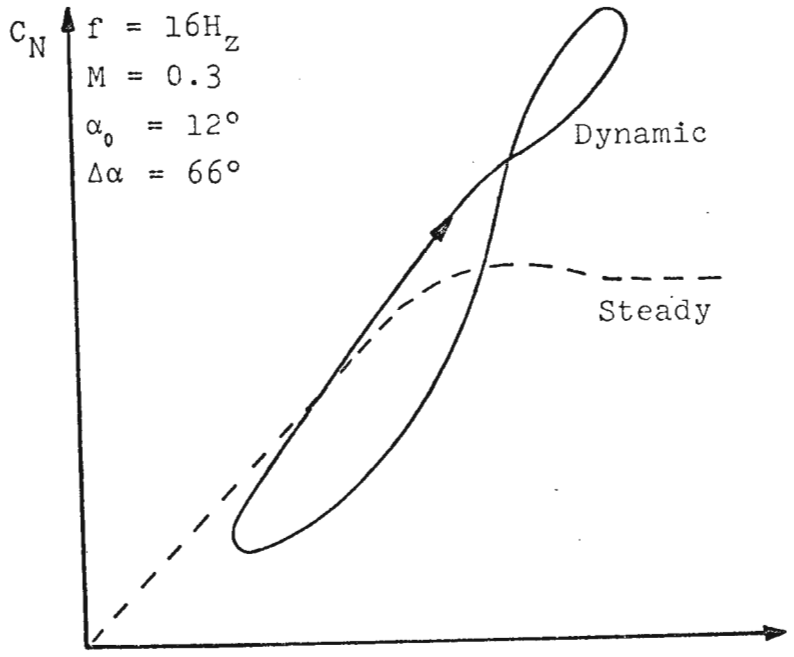

(b)

Figure 6. Unsteady Normal Force Loops

(adapted from Ref. 29)

They concluded that the trailing vortices of a cascade have a mutual cancellation effect.

It should be pointed out that this discussion was based on unsteady effects due to pressure distortions. To readily generalize these effects to the TFG case may result in inaccurate conclusions. This is an area where experimental TFG data would provide an increased understanding of the phenomenon of unsteady, TFG flow.

B. CASCADE SECONDARY FLOW

A definition of secondary flow in turbomachines is that it is the difference between the actual flow and the idealized axisymmetric flow [Ref. 34]. It has been estimated that for high specific energy compressors up to 80% of the loss in total pressure is attributable to secondary flow effects [Ref. 35]. Figure 7 is a qualitative representation of most of the components of secondary flow and the resulting vorticity. It is easy to see why accurate prediction of the aerodynamic influence of a cascade alone has not been achieved [Ref. 30]. In considering the effects of inlet TFG distortion on secondary flow, attention will be focused on those components of vorticity modified by turning the flow.[1]

Squire and Winter [Ref. 37] developed a model for steady, incompressible and inviscid flow which treated the secondary flow as a linear perturbation superposed on the main flow.

---

[1]For a state of the art report on the analytical treatment of secondary flows, see Woods [Ref. 34].

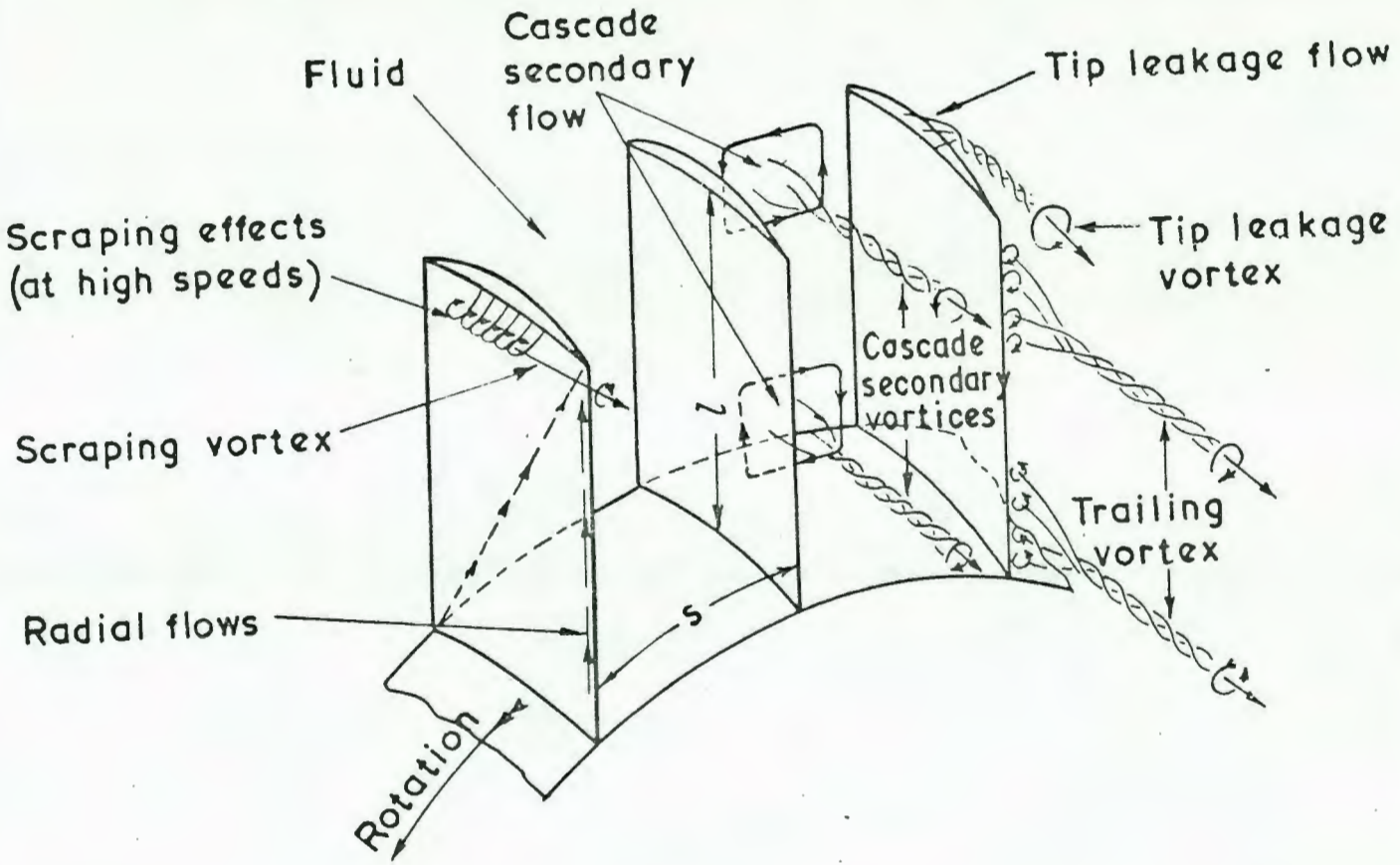

Figure 7. Secondary Flow and Vortices in an Axial Flow Compressor Rotor (adapted from Ref. 36)

Applying linear theory, they were able to show the generation of a streamwise vorticity component when inlet vorticity normal to the streamtube is turned by a passage. Hawthorne [Ref. 38] extended the turning effects to include trailing filament vorticity and trailing shed vorticity. The former is due to stretching of the vortex filaments between the upper and lower stagnation streamline (Fig. 8). The latter is due to the change in circulation along the blade. The net value of secondary vorticity is the sum of these effects. Section VI will present an analysis of the Squire and Winter effect.

Again, it is worthy of note that these secondary flow effects are due to vorticity. A search of the available literature indicates a need for study of secondary flows resulting from TFG distortions.

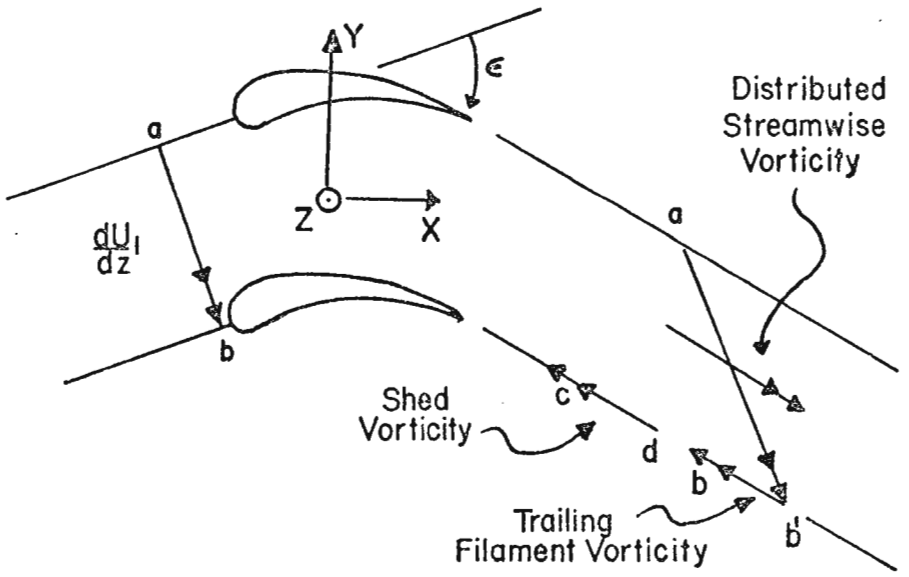

Figure 8. Vortex Filament Passage through a Cascade

(adapted from Ref. 13)

IV. VORTICITY FROM TFG DISTORTION

A. DERIVATION OF MODEL

By proper choice of coordinate system and some simplifying assumptions, it is a straightforward matter to develop a relationship among vorticity, temperature, and pressure which is valid for a mixture of perfect gases. Such a development is presented in Appendix A. For a dual perfect gas system the result in natural coordinates is

$$U\omega = \frac{dh_t}{dn} + \frac{1}{\rho}\frac{\partial P}{\partial n} - \frac{\partial h}{\partial n} \quad . \tag{1}$$

Since this equation does apply to a mixture, enthalpy is defined as $h = C_p T$ where C_p is the specific heat of the mixture. In the majority of cases involving TFG distortion, the inlet is exposed to a non-homogeneous mixture (i.e. there are spatial gradients in the components of the mixture). Thus there will be gradients in C_p. This clearly differentiates the case of one component (i.e. air) and two components (i.e. air and steam).

Equation (1) can be derived in a much more general format. In vector notation the continuity equation is

$$\frac{\partial P}{\partial t} + \vec{\nabla}\cdot(\rho\vec{U}) = 0 \quad .$$

For inviscid flow the equation of motion is

$$\frac{D\vec{U}}{Dt} = \frac{\partial\vec{U}}{\partial t} + (\vec{U}\cdot\vec{\nabla})\,\vec{U} = -\frac{1}{\rho}\vec{\nabla}\,P \quad . \tag{2a}$$

A vector identity is

$$\vec{\nabla}(\tfrac{1}{2}\vec{U}\cdot\vec{U}) = (\vec{U}\cdot\vec{\nabla})\vec{U} + \vec{U}\times(\vec{\nabla}\times\vec{U}) \qquad (2b)$$

where $\vec{\nabla}\times\vec{U} = \vec{\Omega}$ is the vorticity vector. Combining Eqs. (2a) and (2b) yields

$$\frac{\partial\vec{U}}{\partial t} - \vec{U}\times\vec{\Omega} + \vec{\nabla}(\tfrac{1}{2}\vec{U}\cdot\vec{U}) = -\frac{1}{\rho}\vec{\nabla}P \; . \qquad (2c)$$

From the definition of total enthalpy

$$\vec{\nabla}h_t = \vec{\nabla}(\tfrac{1}{2}\vec{U}\cdot\vec{U}) + \vec{\nabla}h \; . \qquad (2d)$$

Introducing Eq. (2d) into (2c) results in

$$\vec{U}\times\vec{\Omega} = \vec{\nabla}h_t + \frac{1}{\rho}\vec{\nabla}P - \vec{\nabla}h + \frac{\partial\vec{U}}{\partial t} \; . \qquad (3)$$

For steady flow this reduces to Eq. (1). Equation (3) is the model to be used to determine flow vorticity. The assumptions involved in deriving this model are:

Inviscid Flow

Perfect Gases

Entropy Constant Along Streamlines.

B. VORTICITY IN INCOMPRESSIBLE FLOW

The isentropic relationship

$$\frac{P_t}{P} = \left(1 + \frac{\gamma-1}{2}M^2\right)^{\frac{\gamma}{\gamma-1}}$$

can be expanded to

$$P_t - P = \frac{1}{2}\rho U^2\left(1 + \frac{M^2}{4} + (2-\gamma)\frac{M^2}{24} + \ldots\right)$$

which for small local Mach numbers reduces to

$$P = P_t - \tfrac{1}{2}\rho U^2 . \qquad (4)$$

Introducing Eq. (4) into Eq. (3) results in

$$\vec{U} \times \vec{\Omega} = \frac{1}{\rho} \vec{\nabla} P_t - \tfrac{1}{2}U^2 \vec{\nabla} \ln\rho + \frac{\partial \vec{U}}{\partial t} . \qquad (5)$$

Note that the presence of FG leads to the gradient in density.[1] For a single perfect gas in incompressible flow, the gradient in density disappears leaving vorticity as a function of velocity, total pressure, and the unsteady effects. In terms of experimental data gathering, these factors seem well within the scope of present techniques. However, the addition of FG to the flow creates a complex relationship.

C. VORTICITY IN COMPRESSIBLE FLOW

Expanding Eq. (3)

$$\vec{U} \times \vec{\Omega} = T_t \vec{\nabla} C_p + C_p \vec{\nabla} T_t + \frac{1}{\rho} \vec{\nabla} P - T \vec{\nabla} C_p - C_p \vec{\nabla} T + \frac{\partial \vec{U}}{\partial t} .$$

This reduces to

$$\vec{U} \times \vec{\Omega} = (T_t - T) \vec{\nabla} C_p + C_p (\vec{\nabla} T_t - \vec{\nabla} T) + \frac{1}{\rho} \vec{\nabla} P + \frac{\partial \vec{U}}{\partial t} . \qquad (6)$$

For the special case of one gas, the first term on the right side would vanish. But for the general case of both temperature and foreign gas, Eq. (6) applies. Appendix C contains a simple application to provide an example as well as an order of magnitude and sign verification.

---

[1] Appendix B contains an example of how this result might be applied.

V. VORTICITY MAPS

A. ORDER OF MAGNITUDE ANALYSIS

The vorticity equation for compressible flow was found to be

$$\vec{U} \times \vec{\Omega} = (T_t - T)\vec{\nabla}C_p + C_p(\vec{\nabla}T_t - \vec{\nabla}T) + \frac{1}{\rho}\vec{\nabla}P + \frac{\partial \vec{U}}{\partial t} . \quad (7)$$

Realizing that a search for compressor inlet mass distribution data would probably be futile, the special case of temperature distortion was considered. The temperature distortion experiment conducted by Rudey and Antl [Ref. 18] was found to closely approximate inlet temperature-only distortion.[1] Thus the flow can be considered to behave as a single gas which reduces Eq. (7) to

$$\vec{U} \times \vec{\Omega} = c_p(\vec{\nabla}T_t - \vec{\nabla}T) + \frac{1}{\rho}\vec{\nabla}P_t + \frac{\partial \vec{U}}{\partial t} . \quad (8)$$

The number of variables can be reduced by eliminating $\vec{\nabla}T$. The procedure involves introducing the combined first and second laws of thermodynamics

$$Tds = dh - \frac{1}{\rho}dP$$

into Eq. (8) resulting in

$$\vec{U} \times \vec{\Omega} = c_p\vec{\nabla}T_t - T\vec{\nabla}s + \frac{\partial \vec{U}}{\partial t} . \quad (9)$$

---

[1] Appendix D contains an analysis to this effect.

This is Crocco's Theorem. From thermodynamics

$$\vec{\nabla}s = \frac{c_p}{T_t}\vec{\nabla}T_t - \frac{R}{P_t}\vec{\nabla}P_t \quad . \tag{10}$$

Combining Eqs. (9) and (10) leads to

$$\vec{U} \times \vec{\Omega} = c_p\vec{\nabla}T_t - \frac{c_p T}{T_t}\vec{\nabla}T_t + \frac{RT}{P_t}\vec{\nabla}P_t + \frac{\partial\vec{U}}{\partial t} \quad .$$

Using the definition of c_p and the isentropic relationship between T_t and T, Eq. (10) can be rearranged to

$$\vec{U} \times \vec{\Omega} = \frac{\gamma RM^2}{2}\left(\frac{1}{1 + \frac{\gamma-1}{2}M^2}\right)\vec{\nabla}T_t + \frac{RT}{P_t}\vec{\nabla}P_t + \frac{\partial\vec{U}}{\partial t} \tag{11}$$

For this analysis, an order of magnitude (ε) is defined as

$$\varepsilon = \frac{T_t - \bar{T}_t}{\bar{T}_t} \quad .$$

From Fig. 9 the maximum value for T_t is 590°R. The mean temperature is approximately 520°R. Thus $0(\varepsilon) = 0.13$. For the complete map, $-0.13 \leq \varepsilon \leq +0.13$.

Returning now to Eq. (11) and examining the coefficient of $\vec{\nabla}T_t$

$$\frac{\gamma RM^2}{2}\left(\frac{1}{1 + \frac{\gamma-1}{2}M^2}\right) \cong \frac{\gamma RM^2}{2}\left[1 - \frac{\gamma-1}{2}M^2 + \left(\frac{\gamma-1}{2}M^2\right)^2 - \ldots\right].$$

For Mach numbers less than about 0.5, it is apparent that all terms beyond the first are $0(\varepsilon^2)$ or less and are therefore neglected. This leaves

$$\vec{U} \times \vec{\Omega} = \frac{\gamma RM^2}{2}\vec{\nabla}T_t + \frac{RT}{P_t}\vec{\nabla}P_t + \frac{\partial\vec{U}}{\partial t} \quad . \tag{12}$$

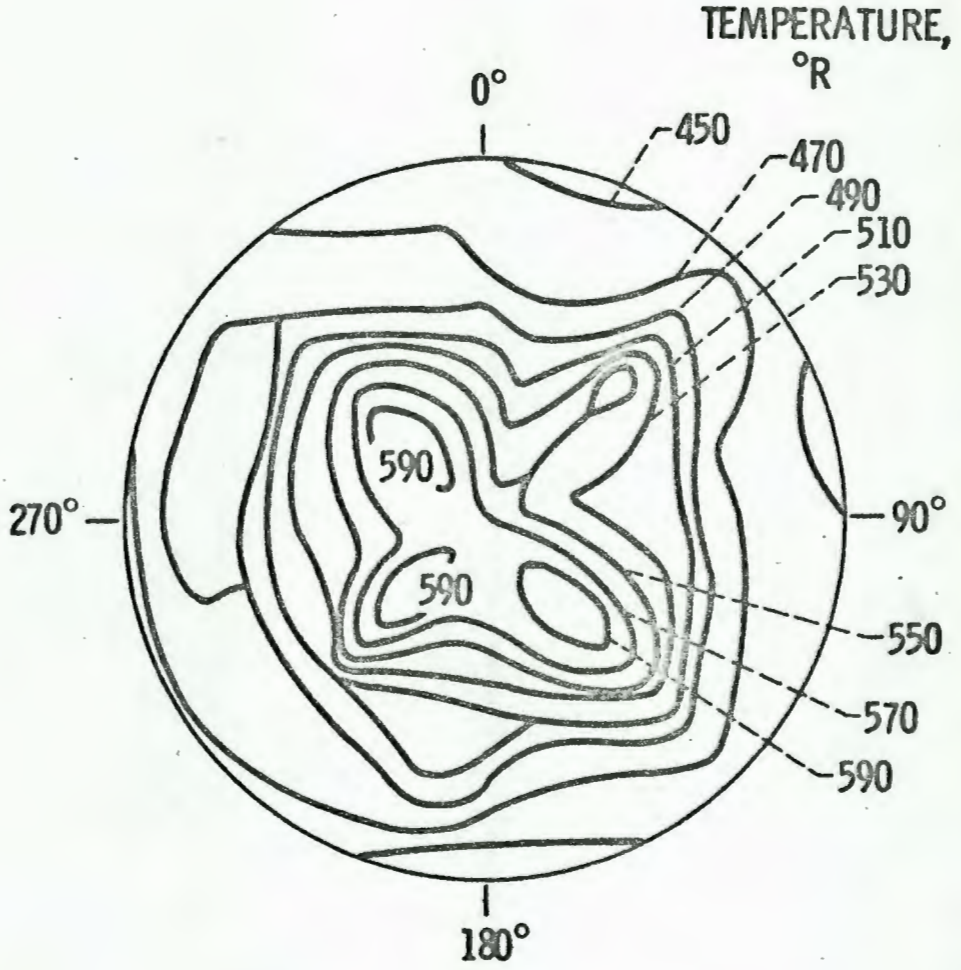

Figure 9. Inlet Temperature Map

(adapted from Ref. 18)

Equation (12) can be written in terms of cylindrical coordinate system components

$$U_\theta \omega_z - U_z \omega_\theta = \frac{\gamma RM^2}{2} \frac{\partial T_t}{\partial r} + \frac{RT}{P_t} \frac{\partial P_t}{\partial r} + \frac{\partial U_r}{\partial t} \quad , \tag{12a}$$

$$U_z \omega_r - U_r \omega_z = \frac{\gamma RM^2}{2r} \frac{\partial T_t}{\partial \theta} + \frac{RT}{P_t r} \frac{\partial P_t}{\partial \theta} + \frac{\partial U_\theta}{\partial t} \quad , \tag{12b}$$

and

$$U_r \omega_\theta - U_\theta \omega_r = \frac{\gamma RM^2}{2} \frac{\partial T_t}{\partial z} + \frac{RT}{P_t} \frac{\partial P_t}{\partial z} + \frac{\partial U_z}{\partial t} \quad . \tag{12c}$$

To non-dimensionalize the vorticity equations, reference quantities were selected at the engine inlet. Based on data from Rudey and Antl [Refs. 18, 39 and 40], the quantities (denoted by a superscript bar) used in this analysis are: 1. $\bar{T}_t$, 520°R; 2. $\bar{T}$, 510°R; 3. $\bar{r}$, 1.5 ft; and 4. $\bar{M}$, 0.4. These reference quantities are used in the following definitions

$$U = U'\bar{a} \qquad P_t = P'_t \bar{P}_t$$

$$\omega = \omega'\bar{a}/\bar{r} \qquad t = t'\bar{r}/\bar{a}$$

$$T_t = T'_t \bar{T}_t \qquad z = z'\bar{r}$$

$$T = T'\bar{T} \qquad r = r'\bar{r} \quad .$$

The superscript prime signifies non-dimensional quantities. Rewriting Eq. (12a) in non-dimensional form

$$U'_\theta \omega'_z - U'_z \omega'_\theta = \frac{M^2}{2} \frac{\bar{T}_t}{\bar{T}} \frac{\partial T'_t}{\partial r'} + \frac{T'}{\gamma P'_t} \frac{\partial P'_t}{\partial r'} + \frac{\partial U'_r}{\partial t'} \quad .$$

Since

$$\frac{\bar{T}_t}{\bar{T}} = 1 + \frac{\gamma - 1}{2} \bar{M}^2 \cong 1 + O(\varepsilon^2) \cong 1 \quad ,$$

the non-dimensional form becomes

$$U'_\theta \omega'_z - U'_z \omega'_\theta = \frac{M^2}{2} \frac{\partial T'_t}{\partial r'} + \frac{T'}{\gamma P'_t} \frac{\partial P'_t}{\partial r'} + \frac{\partial U'_r}{\partial t'} \quad . \tag{13a}$$

Equations (12b) and (12c) are similarly transformed into

$$U'_z \omega'_r - U'_r \omega'_z = \frac{M^2}{2r'} \frac{\partial T'_t}{\partial \theta} + \frac{T'}{\gamma P'_t r'} \frac{\partial P'_t}{\partial \theta} + \frac{\partial U'_\theta}{\partial t'} \tag{13b}$$

and

$$U'_r \omega'_\theta - U'_\theta \omega'_r = \frac{M^2}{2} \frac{\partial T'_t}{\partial z'} + \frac{T'}{\gamma P'_t} \frac{\partial P'_t}{\partial z'} \quad \frac{\partial U'_z}{\partial t'} \quad . \tag{13c}$$

An order of magnitude for $\partial T'_t/\partial r'$ can be established using Fig. 9. At the 8 o'clock position, the value for $\Delta T'_t/\Delta r'$ is 2.5 or $0(\varepsilon^\circ)$. Likewise, $\partial T'_t/(r'\partial\theta)$ can be evaluated at the 2 o'clock position. There, $\Delta T'_t/(r'\Delta\theta)$ was calculated to be 1.7 or $0(\varepsilon^\circ)$. An approximation of $\partial T'_t/\partial z'$ can be obtained using data from Ref. 18. It was found that the engine inlet experienced temperature changes of up to 8500°R/s. By non-dimensionalizing this rate and dividing by U'_z, the order of $\partial T'_t/\partial z'$ was found to be ε. This involves the assumption that $DT'_t/Dt' = 0$.

The components of vorticity are the unknowns to be determined. They are assigned $0(\varepsilon^\circ)$ subject to later confirmation. Order of magnitude estimates for the remaining terms are generally based on physical considerations, which are now discussed.

The main flow can be considered to be almost totally axial. Thus U'_z is essentially $\bar{M}$ which is $0(\varepsilon)$. The presence of U'_r is caused by streamtube divergence from the heating

process.[1] If the engine inlet is sufficiently far enough downstream that the streamtube divergence approaches equilibrium (i.e. static pressure across a plane normal to the flow is approximately constant), then U_r' is $0(\varepsilon^2)$. This is mathematically shown in Appendix E. If it is assumed that there is small duct swirl, then by applying an argument similar to that of U_r', U_θ' is $0(\varepsilon^2)$.

Evaluation of $\partial U_z'/\partial t'$ term was possible through use of Fig. F-3. Using finite differences between lines of constant velocity at constant z, a value for $\Delta U_z'/\Delta t'$ was computed as 0.006. Since the region of heat addition should also be region of maximum $\Delta U_z'/\Delta t'$, assignment of $0(\varepsilon^2)$ seems reasonable. An evaluation of $\partial U_r'/\partial t'$ and $\partial U'/\partial t'$ was conducted in Appendix E. As a result, they are assigned $0(\varepsilon^2)$.

The term $\partial P_t'/\partial z'$ was evaluated in Appendix F and found to be $0(\varepsilon^2)$. The terms $\partial P_t'/(r'\partial\theta)$ and $\partial P_t'/\partial r'$ are assigned $0(\varepsilon^2)$ based on information from Ref. 40.

A summary of the preceding discussion is presented in Table I. It is reiterated that these results are estimates. Additionally they are applicable only to the flow system under analysis.

Equations (13a, b and c) are rewritten with appropriate orders of magnitude above each term

---

[1] Engine inlet hub effects on U_r' are neglected, since the map of temperature is at a station ahead of the hub.

Table I. Relative Orders of Magnitude

Variable	Order	Comments
ω_r'	ε^o	Assumed
ω_θ'	ε^o	Assumed
ω_z'	ε^o	Assumed
U_r'	ε^2	a. Streamtube divergence due to heating b. Confined by duct
U_θ'	ε^2	a. Streamtube divergence due to heating b. No swirl added in bellmouth c. Swirl size of ε would cause engine to stall
U_z'	ε	Main flow
$\frac{\partial T_t'}{\partial r'}$	ε^o	Fig. 9
$\frac{\partial T_t'}{r' \partial \theta}$	ε^o	Fig. 9
$\frac{\partial T_t'}{\partial t'}$	ε	Fig. F-3
$\frac{\partial U_z'}{\partial t'}$	ε^2	Fig. F-3
$\frac{\partial U_r'}{\partial t'}$	ε^2	Appendix E
$\frac{\partial U_\theta'}{\partial t'}$	ε^2	Appendix E
$\frac{\partial P_t'}{\partial r'}$	ε^2	Ref. 39
$\frac{\partial P_t'}{r' \partial \theta}$	ε^2	Ref. 39
$\frac{\partial P_t'}{\partial z'}$	ε^2	Appendix F
$\frac{M^2}{2}$	ε	
$\frac{T'}{\gamma P_t'}$	ε^o	

$$\underset{\varepsilon^2\varepsilon^0}{U'_\theta\omega'_z} - \underset{\varepsilon\ \varepsilon^0}{U'_z\omega'_\theta} = \underset{\varepsilon}{\frac{M^2}{2}}\ \underset{\varepsilon^0}{\frac{\partial T'_t}{\partial r'}} + \underset{\varepsilon^0}{\frac{T'}{\gamma P'_t}}\ \underset{\varepsilon^2}{\frac{\partial P'_t}{\partial r'}} + \underset{\varepsilon^2}{\frac{\partial U'_r}{\partial t'}} \quad , \tag{13a}$$

$$\underset{\varepsilon\ \varepsilon^0}{U'_z\omega'_r} - \underset{\varepsilon^2\varepsilon^0}{U'_r\omega'_z} = \underset{\varepsilon}{\frac{M^2}{2r'}}\ \underset{\varepsilon^0}{\frac{\partial T'_t}{\partial \theta}} + \underset{\varepsilon^0}{\frac{T'}{\gamma P'_t r'}}\ \underset{\varepsilon^2}{\frac{\partial P'_t}{\partial \theta}} + \underset{\varepsilon^2}{\frac{\partial U'_\theta}{\partial t'}} \quad , \tag{13b}$$

and

$$\underset{\varepsilon^2\varepsilon^0}{U'_r\omega'_\theta} - \underset{\varepsilon^2\varepsilon^0}{U'_\theta\omega'_r} = \underset{\varepsilon}{\frac{M^2}{2}}\ \underset{\varepsilon}{\frac{\partial T'_t}{\partial z'}} + \underset{\varepsilon^0}{\frac{T'}{\gamma P'_t}}\ \underset{\varepsilon^2}{\frac{\partial P'_t}{\partial z'}} + \underset{\varepsilon^2}{\frac{\partial U'_z}{\partial t'}} \quad . \tag{13c}$$

Dropping terms and products of terms of order ε^2 in Eqs. (13a) and (13b) results in

$$-U'_z\omega'_\theta = \frac{M^2}{2}\frac{\partial T'_t}{\partial r'} \tag{14a}$$

and

$$U'_z\omega'_r = \frac{M^2}{2r'}\frac{\partial T'_t}{\partial \theta} \quad . \tag{14b}$$

Since $U'_z \cong M$, the final result becomes

$$\omega'_\theta = -\frac{M}{2}\frac{\partial T'_t}{\partial r'} \tag{15}$$

and

$$\omega'_r = \frac{M}{2r'}\frac{\partial T'_t}{\partial \theta} \quad . \tag{16}$$

Note that for $M = 0.4$ and $\partial T'_t/\partial r' = -2.5$, the corresponding value for ω'_θ is 0.5 which is not $0(\varepsilon^0)$ as previously assumed. What is important is the product of $U'_z\omega_\theta$ is the same order as the product of $(M^2/2)(\partial T'_t/\partial r')$ as seen by

$$(.4)(.5) = (.08)(2.5)$$

$$\varepsilon^{.34}\ \varepsilon^{.45} \cong \varepsilon^{1.22}\ \varepsilon^{-.45}$$

$$\varepsilon^{.79} \cong \varepsilon^{.77} \cong \varepsilon^{1} \quad .$$

Thus the estimates of the individual terms may vary slightly from the actual values. But the hope is that the variance is small. Additional smoothing can be expected from taking products as was seen in this case.

Equations (15) and (16) were employed to convert the temperature map (Fig. 9) into circumferential and radial vorticity maps (Figs. 10 and 11). The streamwise vorticity (ω_z') map could also be developed thru application of the relationship $\text{div}(\vec{\Omega}) = 0$. This enables one to map all three components of vorticity from a two dimensional map; there is, however, an ambiguity in the algebraic sign of ω_z'.

B. DISCUSSION OF RESULTS

Before proceeding, further background concerning this particular temperature distortion induced stall is necessary. Rudey and Antl [Ref. 18] found that the engine stall occurred in the compressor and propagated forward. They attributed this to the fact that the hottest and most rapidly changing temperatures were concentrated in the hub region of the fan. This is the portion of the flow which entered the compressor; whereas, the cooler portions of the flow went through the fan.

The vorticity maps are valid for only one point in time. Nonetheless, they do indicate that significant aerodynamic influence can be expected from the temperature distortion. Negative ω_r' causes the blade circulation to be increased thus increasing blade loading. Positive ω_θ' causes the inner portion of the blade span to experience increased flow

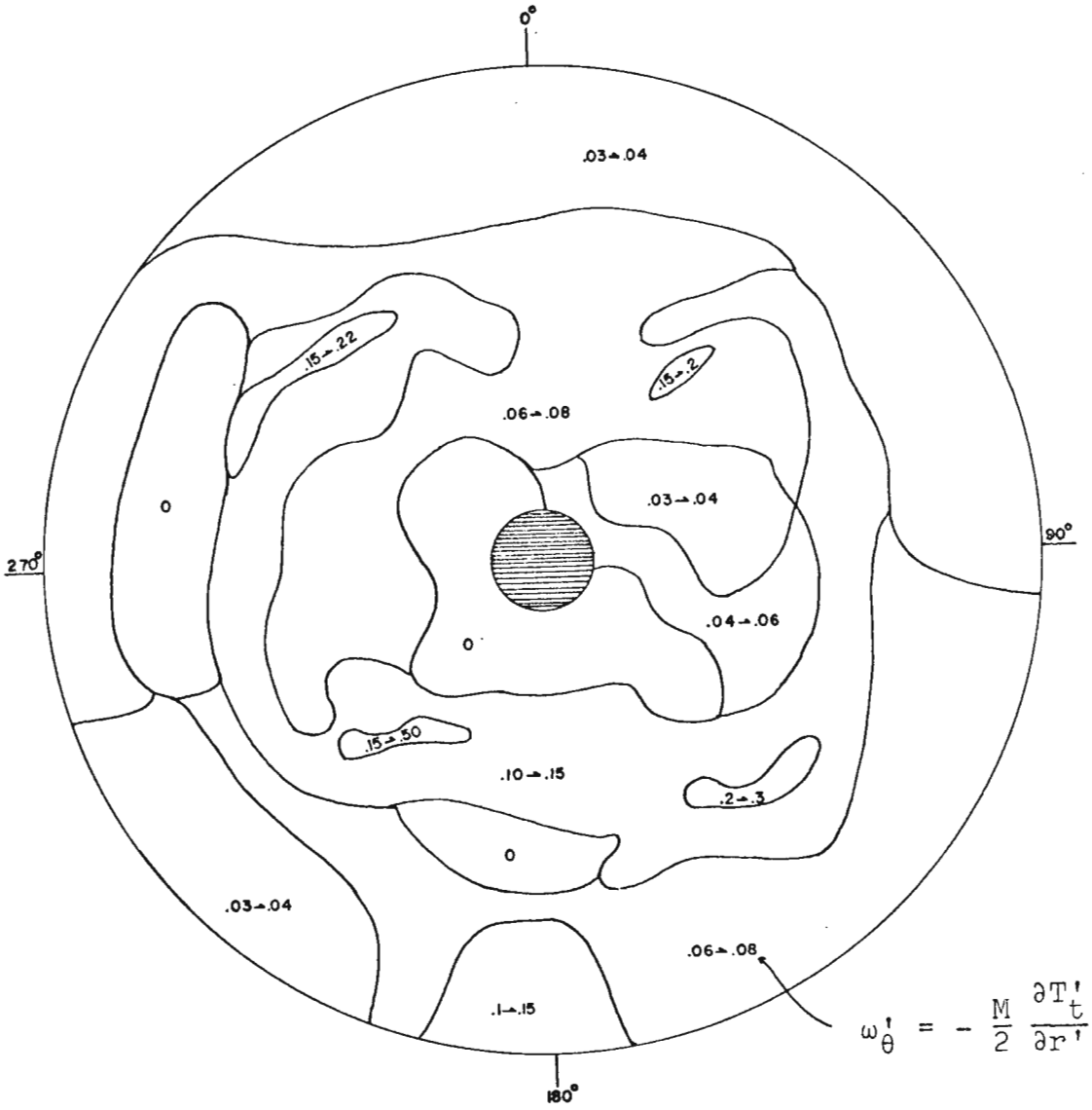

Figure 10. Circumferential Vorticity

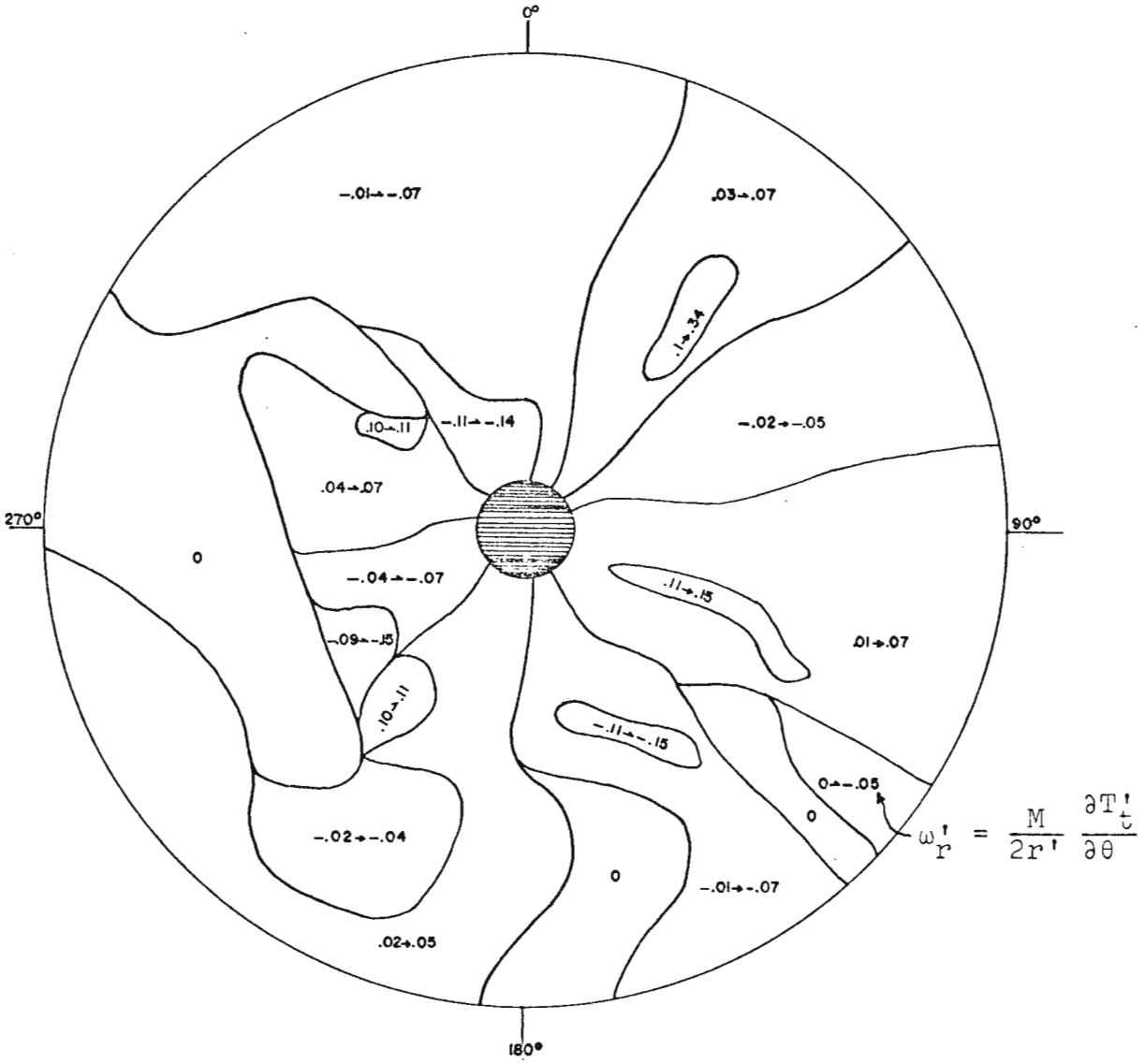

Figure 11. Radial Vorticity

velocities and visa versa. In both cases ω_r' and ω_θ' cause vortex shedding which is probably unsteady. Additionally, associated with ω_θ' is a non-uniform velocity distribution which along with ω_z' causes cascade secondary flow effects.[1] Hence the vorticity approach converts a distortion into aerodynamic terms.

An interesting feature of Fig. 10 is the large ring of ω_θ' at midradii extending from approximately 1 o'clock clockwise around to 12 o'clock. In his study of vorticity due to total pressure distortions, Farmer [Ref. 13] found rings of ω_θ' of approximately the same extent. As will be shown in Section VI, ω_θ' has very definite effects on a cascade. It can therefore be stated that a ring of ω_θ', such as in Fig. 10, is a good indication of instability.

The lack of time history and engine performance data makes further analysis of these maps relative to their role in the engine stall difficult. In addition to the previous time aspect, time history is of importance when considering the transport time of the distortion between the point of measurement and the point where it induces instability. For example, if the instability occurred in the tenth stage and the data gathering took place at the engine inlet, the distortion map of interest probably occurred during the previous ten to fifteen milliseconds. Rudey and Antl [Ref. 18] found the flow breakdown occurred approximately thirty milliseconds

---

[1]For a detailed analysis on inlet vorticity effects, see Farmer [Ref. 13].

after the inlet temperature rise was detected. Figure 9 was recorded about five milliseconds before stall. Since their inlet recording station was about a fan diameter ahead of the compressor, it would probably take fifteen to twenty milliseconds for an inlet distortion to reach the aft stages of the compressor. Based on this estimate, the inlet distortion causing instability occurred ten to fifteen milliseconds before that in Fig. 9. Therefore it is not known whether Fig. 9 is totally representative of the distortion map which was the advent of stall. According to the analysis in Appendix F one would anticipate little change in this time frame.

Data concerning engine performance is necessary to determine such factors as blade loading and estimates of flow turning angles. The former is required to predict effects on changes in blade circulation. It will be shown in the next section that the flow turning angle can be used at least qualitatively to estimate secondary flow losses and, more importantly, onset of stall.

VI. SECONDARY FLOWS DUE TO INLET VORTICITY

A. SECONDARY FLOW MODELS

The analysis of secondary flows has resulted in four flow models - inviscid, viscous, intermediate, and tip clearance [Ref. 34]. The inviscid model is a considerable simplification. Even further simplifications are necessary if Hawthorne's [Ref. 41] result

$$\left(\frac{\xi}{q}\right)_2 - \left(\frac{\xi}{q}\right)_1 = -2\int_1^2 \left| \nabla \frac{P_t}{\rho} \right| \sin\phi \, \frac{d\theta}{q^2} \qquad (17)$$

is to be solved. Hawthorne and Novak [Ref. 42] discuss three classes of approximations required to produce solutions of Eq. (17). They suggested using the assumption of a primary, irrotational flow which convects the vortex filaments. Thus, secondary flow is induced by the convected vorticity. The following discussion utilizes the suggested assumption.

B. POISSON'S EQUATION

Consider the system represented by Fig. 12. From the definition of vorticity, the streamwise component is written

$$\xi_2 = \frac{\partial w}{\partial y} - \frac{\partial v}{\partial z} \quad . \qquad (18)$$

For the assumption of steady vorticity superposed on the mainstream, the induced velocities are defined as $v = \frac{\partial \psi}{\partial z}$ and $w = -\frac{\partial \psi}{\partial y}$ such that continuity $\left(\frac{\partial v}{\partial z} + \frac{\partial w}{\partial y} = 0\right)$ is satisfied. ψ is the stream function. Combining these definitions results in Poisson's equation $\nabla^2\psi = -\xi_2$. The vorticity

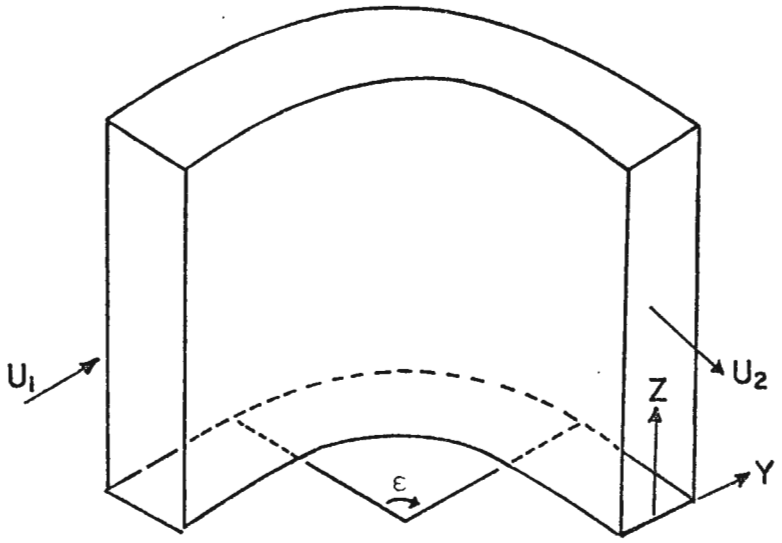

Figure 12. Model of Channel for Cascade Secondary Flow (adapted from Ref. 37)

(ϵ_2) is obtained by solving Eq. (17). The solution of Poisson's equation allows determination of the change in blade circulation $\Delta\Gamma_s$ by [Ref. 42]

$$\Delta\Gamma_s = \int_0^{y_0} v\,dy \ .$$

The change in lift can then be computed by

$$\Delta L = \Delta\Gamma_s \rho U_m$$

where U_m is the vector mean of the velocities of entry and exit, U_1 and U_2 [Ref. 43]. Through application of momentum concepts, the change can be expressed in terms of kinetic energy. However, for the inviscid model the values calculated would be qualitative in nature [Ref. 44]. Thus a solution of Poisson's equation only provides insight into secondary flow losses.

C. APPLICATION OF POISSON'S EQUATION

In order to illustrate the effects of secondary flow, a solution to Poisson's equation was obtained. In so doing, it was necessary to determine values for ξ_2. One approximation often used in the literature is the Squire and Winter [Ref. 37] expression

$$\xi_2 = -2\varepsilon \frac{dU}{dz} \quad . \tag{19}$$

In Eq. (19), ε is the turning angle and U is the inlet velocity. The assumptions underlying this expression are:

Steady, incompressible, inviscid flow

Rectangular channel with $z_{max} \gg y_{max}$

Inlet velocity variation (vorticity) a function of z only

Radius of curvature of the channel is large

Induced velocities are perturbations on the main stream

Despite these assumptions the results obtained by Squire and Winter were very satisfactory. In fact Eq. (19) can be applied to impulse turbines with reasonable accuracy [Ref. 42].

Due to the uncertainty in the results of Section V another flow situation was chosen. Farmer [Ref. 13] obtained vorticity maps of a General Electric J85 undergoing stall due to pressure inlet distortions. It was shown in Section IV that single gas, incompressible flows with temperature distortions can be treated as pressure distortion problems. Thus there is little loss of generality in using Farmer's

work. Figure 13 shows a circumferential vorticity contour map computed by Farmer indicating the radial of interest.

Since the J85 engine has annular cascades and rotors with varying stagger angle and tip clearances, three additional and very coarse approximations were made. First, the annular cascade was approximated by a rectangular cascade. Second, the varying stagger angle was replaced by a mean stagger angle. Third, blade tip losses were excluded. These assumptions were necessary to remain within the confines of the Squire and Winter expression.

The solution of Poisson's equation was obtained by using numerical methods on a digital computer. Appendix G presents the problem formulation and method of solution. There are presently available several computer routines which can be employed in more general flow situations. Hawthorne and Novak [Ref. 42] present a brief summary of the routines available at the writing of their article.

D. DISCUSSION OF RESULTS

The stream function (ψ) distribution is listed in Table II. Examination of the change between the first and second column is equivalent to considering the spanwise induced velocity $w = -\frac{\Delta\psi}{\Delta y}$. Similarly, the change between rows is equivalent to considering the induced downwash $v = \frac{\Delta\psi}{\Delta z}$. Qualitative analysis of these data results in a streamwise vorticity distribution as shown in Fig. 14.

These vorticies have two effects. First, the Biot-Savart law requires that their influence be felt by the

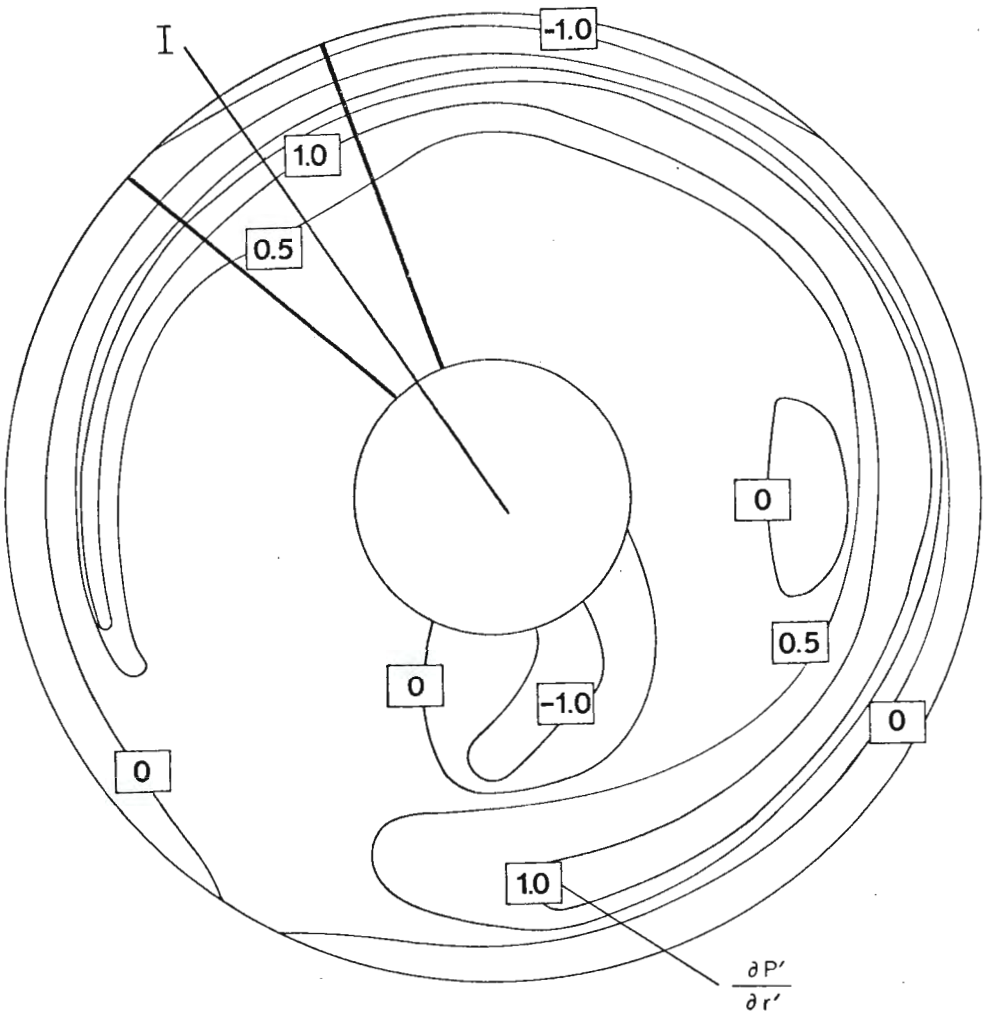

Figure 13. Circumferential Vorticity Contours, J85

(adapted from Ref. 13)

THE PSI DISTRIBUTION

(READ ROW-WISE. FIRST VALUE IS FOR Z= 0.111 AND Y= 0.111)

-15.6	-25.0	-30.6	-33.7	-34.7	-33.7	-30.6	-25.0	-15.6
-24.1	-40.2	-50.5	-56.2	-58.1	-56.2	-50.5	-40.2	-24.1
-29.2	-49.7	-63.3	-71.1	-73.6	-71.1	-63.3	-49.7	-29.2
-32.1	-55.4	-71.3	-80.5	-83.5	-80.5	-71.3	-55.4	-32.1
-33.5	-58.5	-75.8	-85.9	-89.2	-85.9	-75.8	-58.5	-33.5
-34.3	-60.2	-78.3	-88.9	-92.4	-88.9	-78.3	-60.2	-34.3
-34.3	-60.5	-79.0	-89.9	-93.5	-89.9	-79.0	-60.5	-34.3
-34.1	-60.2	-78.8	-89.8	-93.4	-89.8	-78.8	-60.2	-34.1
-33.6	-59.5	-77.9	-88.9	-92.6	-88.9	-77.9	-59.5	-33.6
-33.0	-58.6	-76.8	-87.7	-91.3	-87.7	-76.8	-58.6	-33.0
-32.3	-57.5	-75.4	-86.1	-89.7	-86.1	-75.4	-57.5	-32.3
-31.7	-56.4	-74.0	-84.6	-88.1	-84.6	-74.0	-56.4	-31.7
-31.1	-55.3	-72.7	-83.1	-86.6	-83.1	-72.7	-55.3	-31.1
-30.6	-54.5	-71.5	-81.8	-85.2	-81.8	-71.5	-54.5	-30.6
-30.1	-53.6	-70.5	-80.6	-83.9	-80.6	-70.5	-53.6	-30.1
-29.7	-52.9	-69.5	-79.5	-82.9	-79.5	-69.5	-52.9	-29.7
-29.4	-52.4	-68.8	-78.7	-82.0	-78.7	-68.8	-52.4	-29.4
-29.2	-51.9	-68.2	-78.0	-81.3	-78.0	-68.2	-51.9	-29.2
-28.9	-51.5	-67.6	-77.4	-80.6	-77.4	-67.6	-51.5	-28.9
-28.8	-51.3	-67.4	-77.2	-80.4	-77.2	-67.4	-51.3	-28.8
-28.8	-51.3	-67.6	-77.3	-80.6	-77.3	-67.6	-51.3	-28.8
-28.9	-51.7	-68.0	-77.9	-81.2	-77.9	-68.0	-51.7	-28.9
-29.2	-52.2	-68.9	-78.9	-82.3	-78.9	-68.9	-52.2	-29.2
-29.7	-53.2	-70.3	-80.7	-84.1	-80.7	-70.3	-53.2	-29.7
-30.6	-55.1	-72.8	-83.6	-87.2	-83.6	-72.8	-55.1	-30.6
-32.2	-58.0	-76.8	-88.2	-92.0	-88.2	-76.8	-58.0	-32.2
-34.8	-62.6	-82.8	-94.9	-99.0	-94.9	-82.8	-62.6	-34.8
-39.0	-69.5	-91.4	-104.5	-108.9	-104.5	-91.4	-69.5	-39.0
-43.5	-76.9	-100.6	-114.6	-119.3	-114.6	-100.6	-76.9	-43.5
-47.4	-83.2	-108.4	-123.3	-128.2	-123.3	-108.4	-83.2	-47.4
-50.1	-87.7	-113.9	-129.3	-134.4	-129.3	-113.9	-87.7	-50.1
-51.4	-89.7	-116.2	-131.8	-136.9	-131.8	-116.2	-89.7	-51.4
-50.9	-88.6	-114.6	-129.9	-134.9	-129.9	-114.6	-88.6	-50.9
-47.9	-83.5	-108.0	-122.4	-127.1	-122.4	-108.0	-83.5	-47.9
-42.8	-74.8	-97.0	-110.0	-114.3	-110.0	-97.0	-74.8	-42.8
-36.7	-64.3	-83.4	-94.6	-98.3	-94.6	-83.4	-64.3	-36.7
-29.9	-52.3	-67.8	-76.9	-79.9	-76.9	-67.8	-52.3	-29.9
-22.1	-38.5	-49.9	-56.7	-58.9	-56.7	-49.9	-38.5	-22.1
-12.8	-22.7	-29.6	-33.7	-35.1	-33.7	-29.6	-22.7	-12.8
-4.0	-7.3	-9.8	-11.2	-11.7	-11.2	-9.8	-7.3	-4.0
4.1	7.1	9.2	10.3	10.7	10.3	9.2	7.1	4.1
12.3	21.6	28.0	31.8	33.0	31.8	28.0	21.6	12.3
21.5	37.1	47.7	53.8	55.8	53.8	47.7	37.1	21.5
29.1	50.1	64.2	72.3	75.0	72.3	64.2	50.1	29.1
35.4	60.7	77.5	87.1	90.2	87.1	77.5	60.7	35.4
39.9	67.8	86.1	96.3	99.6	96.3	86.1	67.8	39.9
42.2	70.7	88.6	98.4	101.5	98.4	88.6	70.7	42.2
42.3	67.9	83.1	91.1	93.6	91.1	83.1	67.9	42.3
31.7	48.4	57.5	62.1	63.6	62.1	57.5	48.4	31.7

Table II.

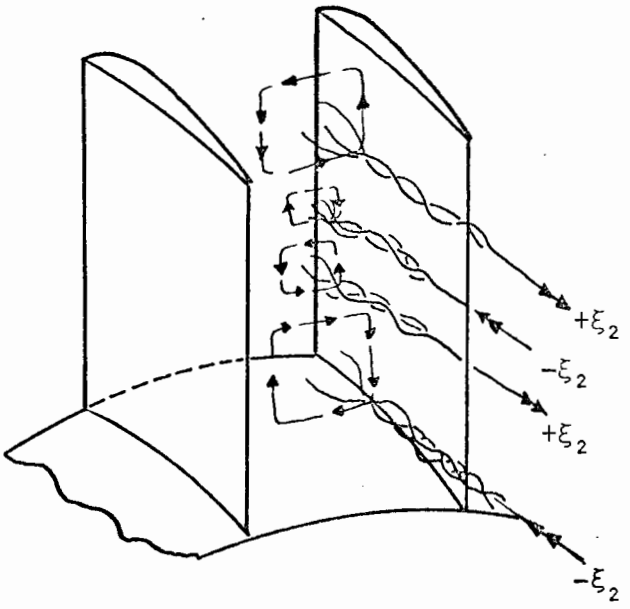

Figure 14. Cascade Secondary Vortices

Due to ω_θ' Inlet Distortion

circulation round the blades of the inducing passage. This is shown in Fig. 15 where their induced downwash is plotted. Note the decreased downwash over the outer portion of the blade. This characteristic of the flow decreases that section's angle of attack. The second effect occurs as the shed vorticies are swept downstream where they will influence the succeeding stages.

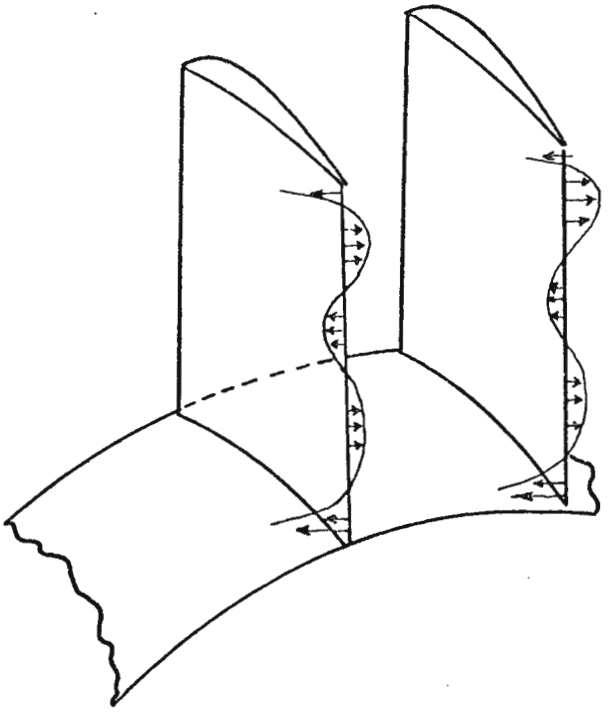

Figure 15. Induced Downwash

VII. SUMMARY

The phenomenon of TFG distortion has been discussed from the vorticity viewpoint. This approach provides insight into the aerodynamic influence associated with TFG distortion. A pure temperature distortion problem was analysed using a temperature map recorded just prior to engine stall. An order of magnitude evaluation of the vorticity equations reduced them to their essential terms. Evaluation of these terms provided data from which vorticity maps were constructed. It was found that by themselves the maps provided some pertinent results which enabled limited analysis to be made. However, to derive full benefit from vorticity analysis, time history and engine performance data were found necessary.

The technique used to develop the vorticity maps was strictly manual in nature. There seems to be great promise if this process could be generalized into a computer program. The main benefit would be labor savings which in turn would allow time history temperature or pressure maps to be converted into time history vorticity maps.

The discussion surfaced various voids of knowledge. For example the effects of unsteady flow and cascade secondary flow in a TFG environment are seemingly unknown. The equations of vorticity require flow density or concentration

maps which are generally not being considered in current TFG studies.[1]

The idea of the aerodynamic transfer function summarizes one suggested use of the vorticity approach. This is because if one combines the compressor stage's design characteristics with its aerodynamic response characteristics, the stage transfer function is defined. Vorticity is the initial input. Figure 16 illustrates this point. D_{0-1} is the vorticity impressed on the engine inlet. The stage transfer function is G_1. As a result D_{0-1} is transformed into D_{1-2} - the distortion from the first stage being impressed on the second stage. Note the feedback loop which

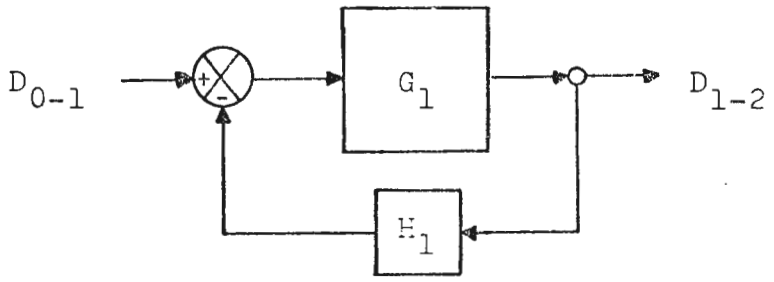

Figure 16. Block Diagram for Aerodynamic Transfer Function

---

[1]It is recognized that collection of flow density data presents a problem. In most experiments this problem has been glossed over by considering total compressor or engine response. The fact is this does not attack the problem of determining what is aerodynamically happening to the blades or cascades.

would likely be present in subsonic flow. Granted, this is conceptually easy to visualize and extremely difficult to implement. But with vorticity one has an aerodynamically compatible input with which to visualize and analyze inlet TFG distortions.

VIII. CONCLUSIONS

As a result of this study, the heretofore abstract inlet temperature map is now a versatile tool in the analysis of temperature-induced instabilities in an axial flow compressor. The vorticity concept provides answers to questions like "How is the blade circulation being altered?" and "What sort of secondary flow effects can be expected?" Answers to both questions can be found through respectively radial and circumferential vorticity. Mathematically a third component, namely axial vorticity, can be obtained from a two-dimensional map.

To optimize this technique, additional efforts are required. The vorticity equations should be generalized to cope with flow situations involving chemical reactions or phase changes. The effects of TFG on current unsteady airfoil theory and cascade secondary flow theory require investigation. Flow density mapping procedures need to be developed. The latter two areas would not only benefit the vorticity concept but would enhance the general understanding of the TFG problem.

The vorticity concept leads to the idea of an aerodynamic transfer function. In turn, this transfer function is a move in the direction of the ultimate goal - prediction of flow of an arbitrary compressor with arbitrary inlet flow.

APPENDIX A

Derivation of TFG Vorticity Equation

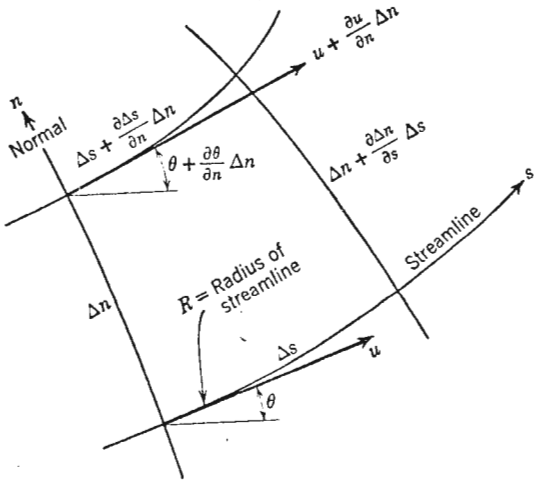

Figure A-1. Natural Coordinate System
(adapted from Ref. 45)

Figure A-1 is an example of the natural coordinate system. This system will be used to develop a general vorticity relationship involving pressure, temperature, and foreign gas. The development will follow that of Liepmann and Roshko [Ref. 45] with the modification of presence of foreign gas.

When a steady, two-dimensional, inviscid, adiabatic flow of a non-homogeneous mixture of perfect gases is considered, the equations of motion are

$$\rho U \Delta n = \text{constant}, \tag{A-1}$$

$$\frac{\partial P}{\partial s} = - \rho U \frac{\partial U}{\partial s} , \tag{A-2}$$

and

$$\frac{\partial P}{\partial n} = - \rho \frac{U^2}{R} \quad . \tag{A-3}$$

By definition

$$h_t = h + \frac{1}{2} U^2 \tag{A-4}$$

Equation A-1 represents continuity for a unit width streamtube. Equations A-2 and A-3 are respectively s and n momentum balance. Equation A-4 is the "energy" equation where by definition stagnation enthalpy is constant along any streamline.

If m_i represents the mass per unit volume of the i^{th} perfect gas at any given point, then let

$$M = \sum_1^n m_i \quad , \qquad \text{(total mass/unit volume)}$$

$$x_i = m_i/M \quad , \qquad \text{(mass fraction)}$$

$$g_i = \frac{\partial x_i}{\partial s} \quad ,$$

and

$$f_i = \frac{\partial x_i}{\partial n}$$

The first two equations are definitions. The second two equations are arrived at by assuming gradients in the n and s direction of the mass fraction of each gas.

For mixtures of perfect gases, the second law of thermodynamics holds that

$$\bar{S} = \sum_1^n m_i \left(c_{p_i} \ln \frac{T}{T_r} - R_i \ln \frac{P_i}{P_r} + \bar{s}_{r_i} \right) \tag{A-5}$$

where: $\bar{S}$ = entropy of mass M

$\bar{s}$ = specific entropy

Subscript r = reference condition

Superscript bar used to delineate between entropy ($\bar{s}$) and the natural coordinate (s)

In terms of specific entropy, equation A-5 can be rewritten as

$$\bar{s} = \sum_{1}^{n} x_i \bar{s}_i \quad .$$

Thus

$$\frac{\partial \bar{s}}{\partial n} = \sum_{1}^{n} \left(x_i \frac{\partial \bar{s}_i}{\partial n} + \bar{s}_i \frac{\partial x_i}{\partial n} \right) = \sum_{1}^{n} \left[x_i \left(\frac{c_{p_i}}{T} \frac{\partial T}{\partial n} - \frac{R_i}{P_i} \frac{\partial P_i}{\partial n} \right) + \bar{s}_i f_i \right]. \tag{A-6}$$

Similarly for the s direction

$$\frac{\partial \bar{s}}{\partial s} = \sum_{1}^{n} \left[x_i \left(\frac{c_{p_i}}{T} \frac{\partial T}{\partial s} - \frac{R_i}{P_i} \frac{\partial P_i}{\partial s} \right) + \bar{s}_i g_i \right] \quad . \tag{A-7}$$

In most practical cases involving distortion the number of perfect gases can be considered to be two - air and the foreign gas. Considering two species of gas, the following relationships apply

$$x_1 + x_2 = 1 \qquad T_1 = T_2 = T$$

$$P_1 + P_2 = P \qquad f_1 = -f_2$$

$$V_1 = V_2 = V \qquad g_1 = -g_2 \quad .$$

It is emphasized that chemical reactions or phase changes are not included in this formulation.

Equation A-6 can be expanded and rearranged so that

$$\frac{\partial \bar{s}}{\partial n} = f_1 (\bar{s}_1 - \bar{s}_2) + \frac{1}{T} (x_1 c_{p_1} + x_2 c_{p_2}) \frac{\partial T}{\partial n}$$

$$- \frac{x_1 R_1}{P_1} \frac{\partial P_1}{\partial n} - \frac{x_2 R_2}{P_2} \frac{\partial P_2}{\partial n} \quad .$$

By definition

$$x_1 c_{p_1} + x_2 c_{p_2} = C_p \text{ of the mixture and}$$

$$\frac{x_1 R_1}{P_1} = \frac{x_2 R_2}{P_2} = \frac{1}{\rho T} \quad .$$

which leads to

$$T \frac{\partial \bar{s}}{\partial n} = T F_1 (\bar{s}_1 - \bar{s}_2) + C_p \frac{\partial T}{\partial n} - \frac{1}{\rho} \frac{\partial P}{\partial n} \quad . \qquad \text{(A-8)}$$

Similarly, it can be shown Eq. (A-7) becomes

$$T \frac{\partial \bar{s}}{\partial s} = T g_1 (\bar{s}_1 - \bar{s}_2) + C_p \frac{\partial T}{\partial s} - \frac{1}{\rho} \frac{\partial P}{\partial s} \quad . \qquad \text{(A-9)}$$

For a chemically inert, perfect gas mixture where $h = C_p T$ then

$$C_p \frac{\partial T}{\partial n} = \frac{\partial h}{\partial n} - T \frac{\partial C_p}{\partial n} \quad .$$

From Eq. (A-4)

$$\frac{\partial h}{\partial n} = \frac{dh_t}{dn} - U \frac{\partial U}{\partial n} \quad .$$

Thus

$$C_p \frac{\partial T}{\partial n} = \frac{dh_t}{dn} - U \frac{\partial U}{\partial n} - T \frac{\partial C_p}{\partial n} \quad . \qquad \text{(A-10)}$$

By introducing Eqs. (A-3) and (A-10) into Eq. (A-8)

$$T \frac{\partial \bar{s}}{\partial n} = T f_1 (\bar{s}_1 - \bar{s}_2) + \frac{dh_t}{dn} - T \frac{\partial C_p}{\partial n} - U \left(\frac{\partial U}{\partial n} - \frac{U}{R} \right) \quad .$$

In natural coordinates the flow vorticity is defined as

$$\omega = \frac{\partial U}{\partial n} - \frac{U}{R}$$

leaving

$$T \frac{\partial \bar{s}}{\partial n} = Tf_1 (\bar{s}_1 - \bar{s}_2) + \frac{dh_t}{dn} - T \frac{\partial C_p}{\partial n} - U\omega \quad . \tag{A-11}$$

The same procedure applied to Eq. (A-9) results in

$$T \frac{\partial \bar{s}}{\partial s} = Tg_1 (\bar{s}_1 - \bar{s}_2) - T \frac{\partial C_p}{\partial s} \quad .$$

Note that $\partial h_t / \partial s = 0$. Assuming no diffusion, condensation, or chemical reactions

$$g_1 = 0$$

and

$$\frac{\partial C_p}{\partial s} = 0 \quad .$$

The result is then simply

$$T \frac{\partial \bar{s}}{\partial s} = 0 \quad . \tag{A-12}$$

Equation (A-12), which is the result of steady, inviscid, adiabatic flow, indicates that entropy along a streamline is a constant.

By subtracting Eq. (A-8) from Eq. (A-11)

$$\frac{dh_t}{dn} - T \frac{\partial C_p}{\partial n} - C_p \frac{\partial T}{\partial n} - U\omega + \frac{1}{\rho} \frac{\partial P}{\partial n} \quad .$$

This can be reduced to

$$U\omega = \frac{dh_t}{dn} + \frac{1}{\rho} \frac{\partial P}{\partial n} - \frac{\partial h}{\partial n} \tag{A-12}$$

which is the desired result.

APPENDIX B

Vorticity in Incompressible Flow

Consider the system shown in Fig. B-1. Assuming the flow is inviscid, adiabatic and incompressible, Eq. 5 can be applied. The next step is to write the corresponding

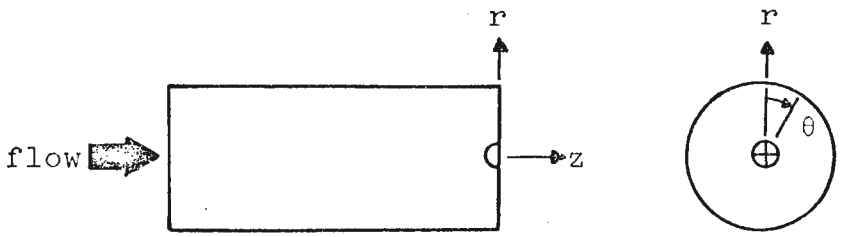

Figure B-1. Flow Model

scalar equations. In this case the cylindrical form was chosen. A suitable scheme should be employed to nondimensionalize the terms. The result might look like

$$U_\theta \omega_z - U_z \omega_\theta = \frac{1}{\rho} \frac{\partial P_t}{\partial r} - \frac{U^2}{2} \frac{\partial \ln \rho}{\partial r} + \frac{\partial U_r}{\partial t} \quad , \tag{B-1}$$

$$U_z \omega_r - U_r \omega_z = \frac{1}{\rho r} \frac{\partial P_t}{\partial \theta} - \frac{U^2}{2r} \frac{\partial \ln \rho}{\partial \theta} + \frac{\partial U_\theta}{\partial t} \quad , \tag{B-2}$$

and

$$U_r \omega_\theta - U_\theta \omega_r = \frac{1}{\rho} \frac{\partial P_t}{\partial z} - \frac{U^2}{2} \frac{\partial \ln \rho}{\partial z} + \frac{\partial U_z}{\partial t} \quad . \tag{B-3}$$

where U is the non-dimensional velocity, ω is the nondimensional vorticity and the subscripts indicate the component

direction. From the initial assumptions

$$\frac{\partial P_t}{\partial z} = 0 \quad \text{and} \quad \frac{\partial \ln \rho}{\partial z} = 0 \quad .$$

One would have a total pressure map (or series of maps) representing the inlet conditions at some event of interest i.e. stall. From this map a maximum and reference pressure ($\overline{P}_t$) could be selected to define an order of magnitude ε

$$\varepsilon = \frac{P_t - \overline{P}_t}{\overline{P}_t} \quad .$$

It becomes a matter of using the available data and/or analyzing the physical flow situation to arrive at orders of magnitude for the components of the equations. For example, if there is small duct swirl (ω_z) and small acceleration in swirl then one might assign the following estimates: 1. $\omega_z = 0(\varepsilon)$; 2. $U_\theta = 0(\varepsilon)$; and 3. $\frac{\partial U_\theta}{\partial t} = 0(\varepsilon)$. From physical considerations the radial component of the flow should generally be negligible with small acceleration. Thus $U_r = 0(\varepsilon^2)$ and $\partial U_r/\partial t$ is $0(\varepsilon)$. The axial velocity (U_z) can be assigned $0(\varepsilon^0)$. The gradients in radial and circumferential pressure can be determined from the pressure map. This procedure would be carried through until all terms had estimates as to their relative order of magnitude. By neglecting terms and products of terms of order ε or less, the equations might look like

$$-U_z \omega_\theta = \frac{1}{\rho} \frac{\partial P_t}{\partial r} - \frac{U^2}{2} \frac{\partial \ln \rho}{\partial r} \quad ,$$

$$U_z \omega_r = \frac{1}{\rho r} \frac{\partial P_t}{\partial \theta} - \frac{U^2}{2r} \frac{\partial \ln \rho}{\partial \theta} \quad ,$$

and

$$-U_\theta \omega_r = \frac{\partial U_z}{\partial t} \quad .$$

Conceptually, these equations now express vorticity in terms of the flow variables. A more detailed procedure is carried through in Ref. 13.

APPENDIX C

Order of Magnitude and Sign Verification of Eq. (6)

Consider the model shown in Fig. C-1 (a).

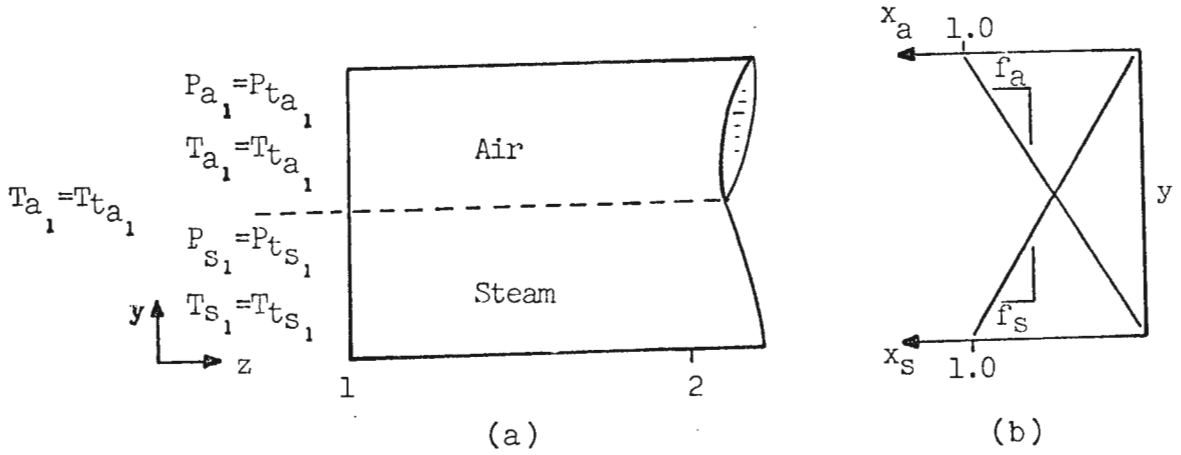

Figure C-1. Flow Model

Assume: (a) Steady, one dimensional, insentropic flow from $1 \rightarrow 2$.

(b) $T_{a_1} = 520°\ R$ $\quad T_{s_1} = 620°\ R$ $\quad \gamma_a = 1.4$

$P_{a_1} = P_{s_1} = 1\ atm$ $\quad P_{a_2} = P_{s_2}$ $\quad \gamma_s = 1.3$

$R_a = 53.3\ \frac{ft - lbf}{lbm - °R}$ $\quad M_{a_2} = 0.5$

$R_s = 85.8\ \frac{ft - lbf}{lbm - °R}$

(c) Linear variations in temperature and mass fraction as depicted in Fig. C-1 (b).

From isentropic tables for $\gamma_a = 1.4$ and $M_{a_2} = 0.5$

$$\frac{P_{a_2}}{P_{t_{a_2}}} = 0.843 \qquad \frac{T_{a_2}}{T_{t_{a_2}}} = 0.952 \ .$$

For isentropic flow, $P_{t_{a_2}} = P_{t_{a_1}} = 1$ atm. and $T_{t_{a_2}} = T_{t_{a_1}}$ $= T_{a_1} = 520°$ R. Therefore, $P_{a_2} = 0.843$ atm. and $T_{a_2} = 495°$ R. From isentropic tables for $\gamma_s = 1.3$ and $P_{s_2}/P_{t_{s_2}} = 0.843$ atm.

$$M_{s_2} = 0.52 \qquad \frac{T_{s_2}}{T_{t_{s_2}}} = 0.961 .$$

Therefore, $T_{s_2} = (.961)(620) = 595°$ R. For speed of sound, $a = (\gamma g_c RT)^{\frac{1}{2}}$. Therefore

$$a_a = \sqrt{(1.4)(32.2)(53.3)(495)} = 1090 \text{ ft/s}$$

$$a_s = \sqrt{(1.3)(32.2)(85.8)(595)} = 1460 \text{ ft/s}$$

The velocities are

$$U_{a_2} = M_{a_2} a_{a_2} = (0.5)(1090) = 545 \text{ ft/s}$$

and

$$U_{s_2} = M_{s_2} a_{s_2} = (0.52)(1460) = 760 \text{ ft/s} .$$

Since the model is for steady planar flow with constant static pressure, Eq. (6) reduces to

$$-\omega U = \frac{dh_t}{dy} - \frac{dh}{dy} .$$

Recall that $C_p = x_a c_{p_a} + x_s c_{p_s}$ and $f_a = dx_a/dy$. Rearranging the above in terms of specific heat and temperature leads to

$$\omega U = f_a (T - T_t)(c_{p_a} - c_{p_s}) + c_p \left(\frac{dT}{dy} - \frac{dT_t}{dy} \right) .$$

In linear and finite difference form

$$-\left(\frac{U_a - U_s}{\Delta y}\right)\left(\frac{U_s + U_a}{2}\right) = \left(\frac{X_a - 0}{\Delta y}\right)\left(\frac{T_{a_2} + T_{s_2}}{2} - \frac{T_{t_{a_2}} + T_{t_{s_2}}}{2}\right)\left(c_{p_a} - c_{p_s}\right)$$

$$+\left(\frac{T_{a_2} - T_{s_2}}{\Delta y} - \frac{T_{t_{a_2}} - T_{t_{s_2}}}{\Delta y}\right)\left(\frac{c_{p_a} + c_{p_a}}{2}\right)$$

which reduces to

$$(U_s^2 - U_a^2) = 2c_{p_a}(T_{a_2} - T_{t_{a_2}}) + 2c_{p_s}(T_{t_{s_2}} - T_{s_2}) \quad .$$

Evaluation with values previously calculated

$$2.8 \times 10^5 \text{ ft}^2/\text{sec}^2 \cong 3.0 \times 10^5 \text{ ft}^2/\text{sec}^2 \quad .$$

The sign is consistent, and the error in this crude approximation is 6.5%.

APPENDIX D

Analysis of Products of Combustion

On a mass basis the chemical equation for the combustion of hydrogen in theoretical air is

$$2.02 \text{ lbm } H_2 + 16.0 \text{ lbm } O_2 + 106 \text{ lbm } N_2$$
$$= 18.02 \text{ lbm } H_2O + 106 \text{ lbm } N_2 \, . \qquad \text{(D-1)}$$

The N_2 term accounts for nitrogen as well as the other inert gases in air. From the data in Ref. 39 the mass flow rate of H_2 for a 150° R change across the heater was computed to be 0.27 lbm/s. The rated air flow of the engine was 186 lbm/s [Ref. 39]. If air into the heater is assumed to be dry, then, based on a one second interval, Eq. (D-1) modified for excess air becomes

$$0.21 \text{ lbm } H_2 + 39 \text{ lbm } O_2 + 147 \text{ lbm } N_2$$
$$= 243 \text{ lbm } H_2O + 36.80 \text{ lbm } O_2 + 147 \text{ lbm } N_2 . \qquad \text{(D-2)}$$

From the results of Eq. (D-2) the specific humidity is found to be 1.3%. Based on that small value, two conclusions were reached: 1. The effects of this humidity on engine performance are negligible [Ref. 46]; and 2. The inlet flow can be considered to be free of foreign gas (water vapor) gradients.

APPENDIX E

Heat Addition in Subsonic Flow

The following equations were developed by Tsien and Beilock [Ref. 47]. For a point heat source in subsonic flow

$$U^* = \frac{(\gamma-1)Q}{2\pi\gamma P\beta} \cdot \frac{x}{x^2+\beta^2y^2} \quad , \tag{E-1}$$

$$V^* = \frac{(\gamma-1)Q}{2\pi\gamma P\beta} \cdot \frac{y}{x^2+\beta^2y^2} \quad , \tag{E-2}$$

and

$$P^* = \frac{(\gamma-1)MQ}{2\pi a\beta} \cdot \frac{x}{x^2+\beta^2y^2} \quad . \tag{E-3}$$

In this notation x and y are analogous to z and r, respectively. Here * indicates a change to the flow variable between the heat source (point 0) and some point (point 1) down (or up) stream. For example, $U_1 = U_0 + U^*$, $P_1 = P_0 + P^*$ etc. Also, $\beta^2 = 1-M^2$, a is the speed of sound and Q is the line source heat addition (BTU/ft-s). If one imposes the requirement that $P^* \cong 0$, then for the non-trivial case x must be large. So, when $P^* \cong 0$, $V^* \cong 0$ and $U^* \cong 0$. Physical considerations lead to the conclusion that U_θ' and U_r' are of the same order as V*. Thus they will necessarily be small.

For the $\partial U_r'/\partial t'$ and $\partial U'/\partial t'$ analysis, Eq. (E-2) can be differentiated with respect to time

$$\frac{\partial V^*}{\partial t} = \frac{\beta}{2\pi} \frac{y}{x^2+\beta^2y^2} \left[\frac{\Delta T}{T} \frac{\partial U_z}{\partial t} + \frac{U_z}{T} \frac{\partial T}{\partial t} \right] .$$

Again, for large x, it can be shown that $\partial V^*/\partial t=0$. Using the same rational as applied to U'_θ and U'_r, $\partial U'_r/\partial t'$ and $\partial U'_\theta/\partial t'$ are small.

APPENDIX F

Order of Magnitude Analysis for a Heat Ramp

The system shown in Fig. F-1 is a constant area duct with heat addition at station 1. Assume the heat source is capable of producing a temperature ramp of 7750° R/s. Suppose

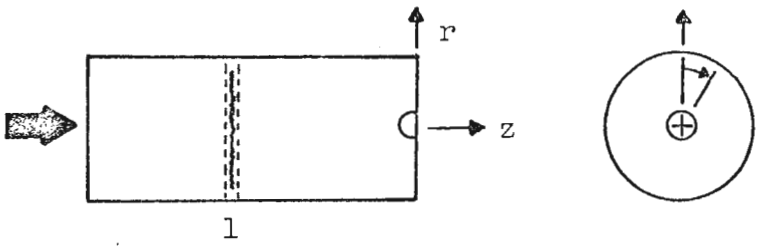

Figure F-1. Heat Ramp Flow Model

one had a case of Rayleigh flow with an impulse change in T_t and a corresponding impulse change in P_t as shown in Fig. F-2(a) and (b).

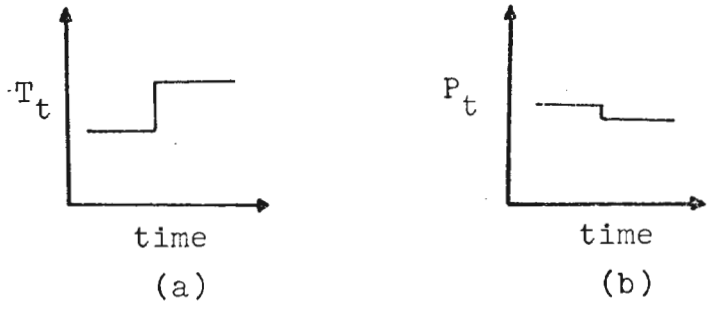

Figure F-2. Impulse Changes in the Flow Variables

The following assumptions are made for the initial conditions: 1. $P = 1$ atm; 2. $M = 0.2$; and 3. $U = 200$ ft/s.

If the flow particles are convected at a velocity U, then changes in pressure propagate at U+a. Changes in temperature due to particle convection propagate at U.

From the assumed initial conditions the following additional initial values can be computed

$$a = U/M = 1000 \text{ ft/s} \quad ,$$

$$T = \frac{a^2}{\gamma g R} = 416^\circ \text{ R} \quad ,$$

and

$$T_t = T_1 (1 + \frac{\gamma-1}{2} M^2) = 419^\circ \text{ R}.$$

At the assumed Mach number the change in T_t can be approximated by the change in T. Thus, between t = 0 and t = 0.01 seconds, $\Delta T_t = 77.5^\circ$ R, etc. Computation of changes in the remaining flow variables during the first 0.01 seconds can be accomplished through the use of thermodynamic influence coefficients

$$\frac{dU}{U} = \frac{1}{1-M^2} \frac{dT_t}{T} = 0.2 \qquad \text{or } U \cong 240 \text{ ft/s}$$

$$\frac{dM}{M} = \frac{1+\gamma M^2}{2(1-M^2)} \frac{dT_t}{T} = 0.1 \quad \text{or } M \cong 0.22$$

$$\frac{dP_t}{P_t} = - \frac{\gamma M^2/2}{1+\frac{\gamma-1}{2} M^2} \frac{dT_t}{T} = - 0.005 \quad \text{or } P_t \cong 0.99 \text{ atm} .$$

In a similar fashion, progressive changes can be computed. Results for the first 0.02 seconds are listed in Table F-I.

This is an approximate analysis; the correct method would involve use of wave techniques outlined by Rudinger [Ref. 48].

Table F-I.

Time Changes in Flow Variables

time	U	M	a	T	T_t	P_t
0	200	.2	1000	416	419	1.0
0.01	240	.22	1090	494	497	0.99
0.02	274	.24	1172	572	575	0.98

It is observed that with respect to time the changes in velocity and temperature are in order of magnitude ten times that of pressure.

From the values in Table F-I, Fig. F-3 was constructed. The slope of the lines are the reciprocal of the transport velocity. In this case the changes are with respect to distance. Again it is obvious that the changes in pressure are negligible. Hence, it can be concluded that for a temperature ramp process the resulting gradient in pressure is negligible.

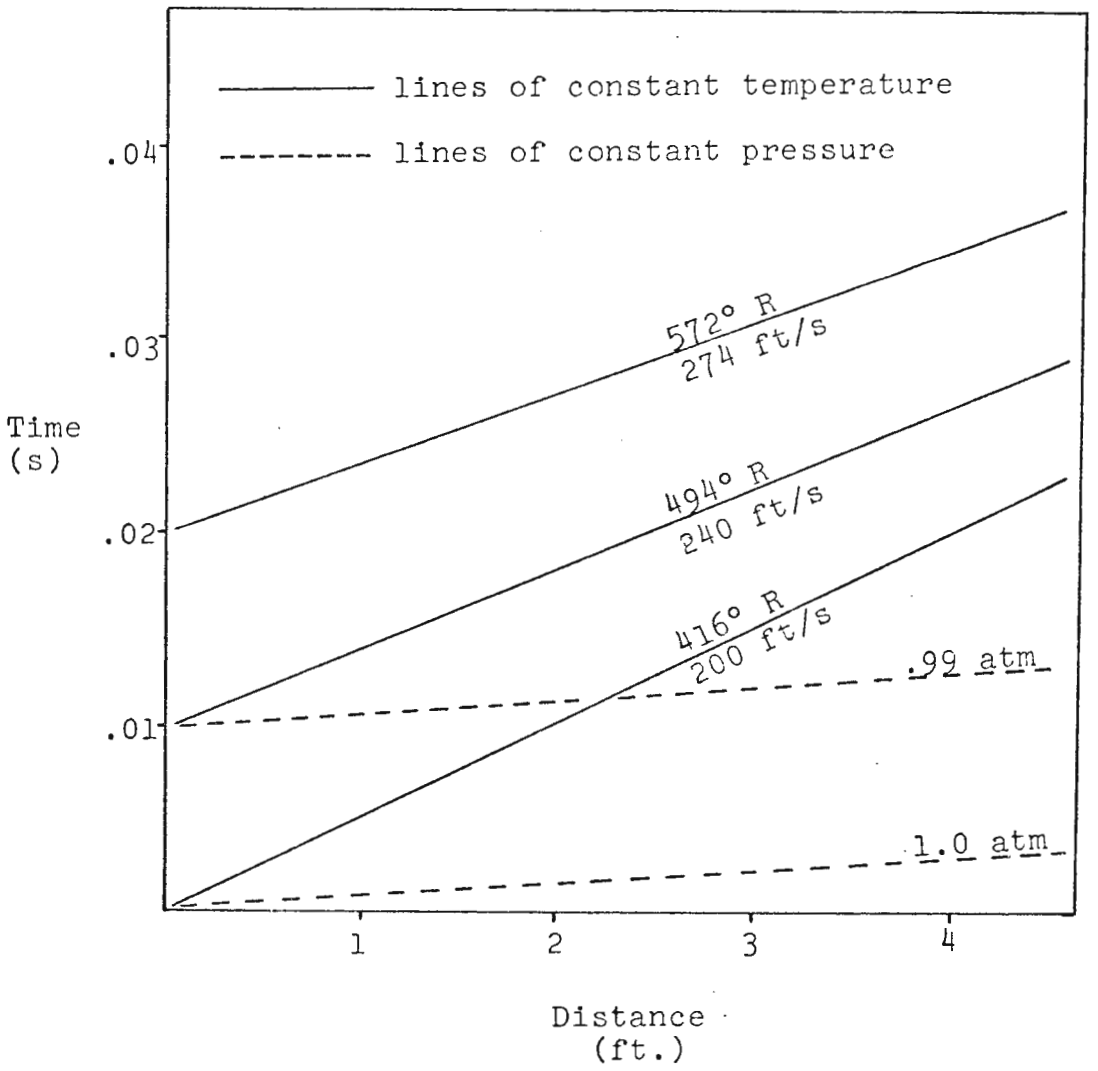

Figure F-3. Transport Characteristics

APPENDIX G

Numerical Solution of Poisson's Equation

Poisson's equation is an equilibrium problem involving an elliptic operator. The boundary value problem is formulated by a governing equation

$$\nabla^2\psi = 2\varepsilon \frac{dU}{dz} \quad .$$

where ∇^2 is the Laplacian operator, ψ is the stream function, ε is the turning angle of the flow and $\frac{dU}{dz}$ is the inlet velocity distortion. The boundary conditions are $\psi = 0$ at $y = 0$, $y = y_{max}$, $z = 0$ and $z = z_{max}$. In using inlet circumferential vorticity the governing equation is modified to

$$\nabla^2\psi = - 2\varepsilon\omega_\theta$$

since by definition $\omega_\theta = - \frac{dU}{dz}$.

The solution technique involves "discretizing" the domain and writing finite difference approximations for the continuous derivatives. These are the standard techniques described in most numerical methods texts.

In matrix notation the general result of the finite difference operations is

$$[D]\{\psi\} = - 2\varepsilon\{\omega_\theta\} \quad .$$

where [D] is a matrix of finite difference coefficients. The solution is obtained by the linear algebra notation

$$\{\psi\} = - 2\varepsilon[D]^{-1}\{\omega_\theta\} \quad .$$

A unique feature of [D] is that it is a banded matrix. This feature can be exploited thru the use of banded matrix solving subroutines. One such subroutine used in this problem is GELB which is found in the IBM Scientific Subroutine Package [Ref. 49].

To test this program, Squire and Winter's [Ref. 37] experimental data was used. The results are shown in Fig. G-1.

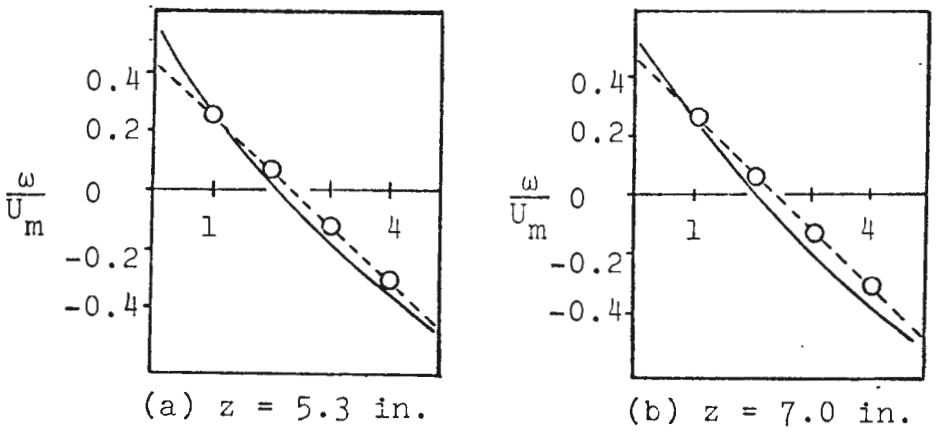

ω = velocity in z direction.

U_m = mean velocity of flow approaching bend.

abscissa = inches from inner vane.

——— Squire and Winter's measurements.

--o-- Numerical solution.

Figure G-1. Comparison of Squire and Winter's Experiment with Numerical Solution

The domain of Farmer's [Ref. 13] J85 problem was modified from Fig. G-2(a) to Fig. G-2(b). The stagger angle which varied from 22° 25' at the hub to 52° 59' at the blade tip

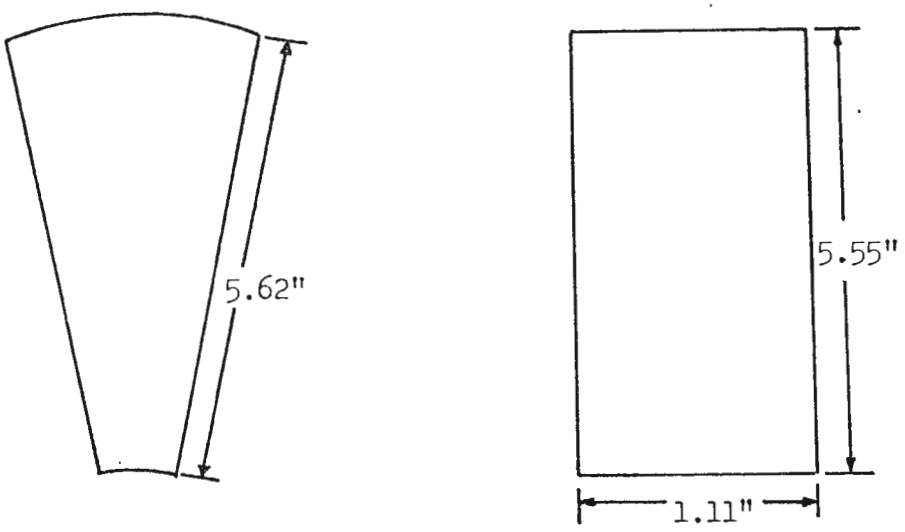

Figure G-2. Actual and Modified Domain for J85 Solution

was replaced by a mean stagger angle of 37° 45'. The turning angle ε was computed by Farmer to be 19°. Values for were computed using the equation obtained from Farmer's paper

$$\omega_\theta = \frac{-2854.9}{P'\sqrt{9.17P' - 8.16}} \cdot \frac{\partial P'}{\partial r'} \quad . \qquad \text{(G-1)}$$

Values for $\partial P'/\partial r'$ and P' were obtained from Fig. 13 along radial I. To obtain the component of ω_θ parallel to the inlet plane (Fig. G-3), the values from Eq. (G-1) were multiplied by cos(37° 45'). The incremental step size was chosen to be 0.111 inches which resulted in a matrix [D] of dimension 49 × 9.

The program appears after the appendices. Since GELB is a standard IBM subroutine it was not included.

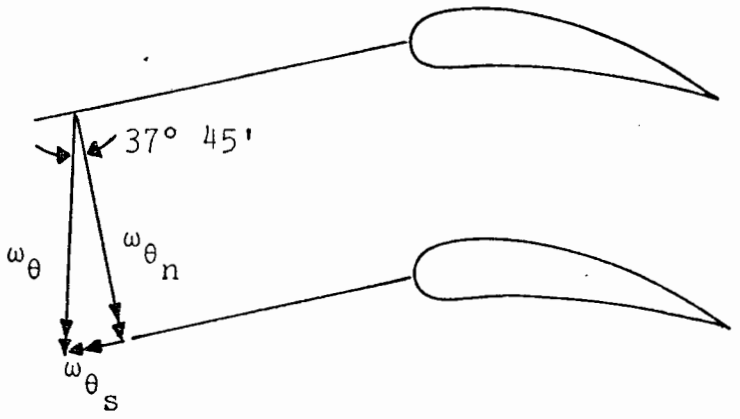

Figure G-3. Components of ω_θ

```
//  EXEC FORTCLG,REGION.GO=76K
//FORT.SYSIN DD DSNAME=SSP3(GELB),DISP=SHR
// DD *
C     ************************************************************
CCC
CCC   NUMERICAL SOLUTION OF POISSON'S EQUATION.
CCC
CCC   DESCRIPTION OF PARAMETERS
CCC      D - VECTOR OF DIMENSION MA CONTAINING COEFFICIENTS
CCC          FROM FINITE DIFFERENCE SCHEME.
CCC   FUNC - VECTOR OF DIMENSION M CONTAINING -2*EPS*WTH.
CCC   WORK - VECTOR OF DIMENSION MUD USED AS A WORKING
CCC          SPACE.
CCC    WTH - VECTOR OF DIMENSION M/MUD.
CCC      M - L/STEP
CCC   STEP - INCREMENT SIZE.
CCC    EPS - FLOW TURNING ANGLE.
CCC   EPSL - A TOLERENCE FOR GELB.
CCC
CCC   REMARKS
CCC      1. FOR DESCRIPTIONS OF THE PARAMETERS MUD, MC, MA,
CCC         ME AND N SEE GELB.
CCC      2. ROW IS ASSOCIATED WITH HEIGHT Z.
CCC         COLUMN IS ASSOCIATED WITH WIDTH Y.
CCC
CCC   ************************************************************
CC
      DIMENSION D(8334),FUNC(441),WORK(19),WTH(49)
      DATA M,MUD,MC,MA,ME,N/441,9,19,8334,8289,1/
      DATA STEP,EPS,EPSL/1.110E-01,1.0E-06,3.3160E-01/
      KZ=M/MUD
C
CCC   READ VALUES FOR OMEGA-THETA.
CC
      READ (5,100) (WTH(J),J=1,KZ)
C
CCC   ECHO CHECK.
C
      WRITE (6,101)
      WRITE (6,107) (WTH(J),J=1,KZ)
C
CCC   FORM THE FUNCTIONAL VECTOR 'FUNC'.
CC
      J=MUD
      JJ=1
      DO 10 I=1,M
      IF(I.LE.J) GO TO 9
      J=J+MUD
      JJ=JJ+1
    9 Z=STEP*JJ
   10 FUNC(I)=-2.0*EPSL*WTH(JJ)*COS(.6555)*STEP*STEP
C
CCC   PRINT 'FUNC' OF EACH ROW.
CC
      WRITE (6,104)
      WRITE (6,103) STEP
      WRITE (6,109) (FUNC(J),J=1,M,9)
      WRITE (6,104)
C
CCC   FORM THE COEFFICIENT VECTOR 'D'.
CC
      CALL LOAD (WORK,D,M,MC,MUD,ME,MA)
C
CCC   SOLVE FOR THE STREAM FUNCTION.
C
      CALL GELB (FUNC,D,M,N,MUD,MUD,EPS,IER)
      IF (IER.EQ.-1) GO TO 99
C
CCC   PRINT STREAM FUNCTION.
CC
      WRITE (6,105) STEP,STEP
```

```
      WRITE (6,106) (FUNC(J),J=1,M)
      GO TO 1000
   99 WRITE (6,108)
  100 FORMAT (7F10.1)
  101 FORMAT ('1',55X,'OMEGA-THETA ECHO CHECK'////)
  102 FORMAT (22X,7F10.1//)
  103 FORMAT (58X,'THE FUNCTIONAL VALUES'//,46X,
     1'(READ ROW-WISE. FIRST VALUE IS FOR Z= ',F5.3,')'////)
  104 FORMAT (////)
  105 FORMAT ('1',53X,'THE PSI DISTRIBUTION'///,36X,
     2'(READ ROW-WISE. FIRST VALUE IS FOR Z= ',F5.3,
     3' AND Y= ',F5.3,')'////)
  106 FORMAT (18X,9F10.1)
  107 FORMAT (29X,9F10.1)
  108 FORMAT (5X,'STOPPED AT GELB')
  109 FORMAT (38X,7F8.1)
 1000 STOP
      END
```

```
C     ***************************************************
C
C     SUBROUTINE LOAD
C
C     PURPOSE
C        TO FORM A VECTOR 'D' OF DIMENSION MC. THIS IS IN
C        LIEU OF BUT IDENTICAL TO FORMING A ROW-WISE MATRIX
C        OF BAND ELEMENTS AS REQUIRED BY GELB.
C
C     DESCRIPTION OF PARAMETERS
C     MOLV - DUMMY NAME GIVEN 'D'.
C      VEC - VECTOR CONTAINING THE ELEMENTS OF THE BAND.
C
C     ***************************************************
C
      SUBROUTINE LOAD (MOLV,VEC,M,MC,MUD,ME,MA)
      REAL MOLV(MC),VEC(MA)
C
C     FORM THE BAND ELEMENT VECTOR 'MOLV'.
C
      DO 10 I=1,MC
      IF((I.EQ.1).OR.(I.EQ.MUD).OR.(I.EQ.MUD+2).OR.(I.EQ.MC)
     1) GO TO 5
      IF (I.EQ.MUD+1) GO TO 7
      MOLV(I)=0.0
      GO TO 10
    5 MOLV(I)=1.0
      GO TO 10
    7 MOLV(I)=-4.0
   10 CONTINUE
C
C     FORM 'MOLV'. THE END BOUNDRY CONDITIONS ARE INCLUDED.
C
      K1=((MUD+MC)/2)*MUD
      IH=0
      II=0
      IJ=MUD
      IK=0
      IL=MC-1
      DO 20 I=1,MA
      IF(I.LE.K1) GO TO 12
      IF((I.GT.ME-K1).AND.(I.LE.ME)) GO TO 15
      IF(I.GT.ME) GO TO 18
C
C     LOAD MIDDLE VEC WITH MOLV.
C
      IH=IH+1
      IF(IH.GT.MC) IH=1
      VEC(I)=MOLV(IH)
      GO TO 20
C
C     LOAD UPPER VEC WITH LOWER MOLV.
C
   12 II=II+1
      IH=IJ+II
      IF(IH.GT.MC) GO TO 13
      VEC(I)=MOLV(IH)
      GO TO 20
   13 II=0
      IJ=IJ-1
      GO TO 12
C
C     LOAD LOWER VEC WITH UPPER MOLV.
C
   15 CONTINUE
      IK=IK+1
      IF(IK.GT.IL) GO TO 17
   16 VEC(I)=MOLV(IK)
      GO TO 20
```

```
   17 IK=1
      IL=IL-1
      GO TO 16
C
C     ZERO REMAINING MA - ME SPACES OF VEC.
C
   18 VEC(I)=0.0
   20 CONTINUE
C
C     INITIALIZE SIDE BOUNDRY CONTITIONS TO ZERO.
C
      KZER1=K1-MUD+1
      KSTEP=MC*MUD
      DO 30 I=KZER1,ME,KSTEP
      VEC(I)=0.0
      KZER2=I+MC-2
   30 VEC(KZER2)=0.0
      RETURN
      END
```

REFERENCES

1. Brimelow, B., Performance Matching of the Propulsion System, SAE preprint 680712, Aeronautics and Space Engineering and Manufacturing Meeting, Los Angeles, Calif., October 1968.

2. NASA TMX-1928, Experimental Investigation of the Effects of Pulse Pressure Distortions Imposed on the Inlet of a Turbofan Engine, by L. M. Wenzel, November 1969.

3. AIAA Paper No. 70-632, Distortion and Turbulence Interaction, A Method for Evaluating Engine/Inlet Compatibility, by E. A. Van Deusan and V. R. Mardoc, June 1970.

4. Plourde, G. A. and Brimelow, B., Pressure Fluctuations Cause Compressor Instability, paper presented at the Airframe/Propulsion Compatibility Symposium, Wright-Patterson AFB, Ohio, 25 June 1969

5. AIAA Paper No. 70-624, Analysis of In-Flight Pressure Fluctuations Leading to Engine Compressor Surge in an F-111A Airplane for Mach Numbers to 2.17, by F. W. Burcham, Jr. and D. L. Hughes, June 1970.

6. AIAA Paper No. 69-488, The Flight Investigation of Pressure Phenomena in the Air Intake of an F-111A Airplane, by D. R. Bellman and D. L. Hughes, 1969.

7. Carta, F. O., "Effect of Unsteady Pressure Gradient Reduction on Dynamic Stall Delay," Journal of Aircraft, v. 8, p. 839-841, 1971.

8. NASA TMX-2239 Experimental Investigation of the Effect of Screen-Induced Total Pressure Distortion on Turbojet Stall Margin, by J. E. Calogeras, C. M. Mehalic, and P. L. Burstadt, Lewis Research Center, Cleveland, Ohio, March 1971.

9. Burcham, F. W. and Bellman, D. R., A Flight Investigation of Steady-State and Dynamic Pressure Phenomena in the Air-Inlets of Supersonic Aircraft, paper presented 38th Meeting of AGARD, Sandefjord, Norway, September 1971.

10. NASA TMX-2081, Effect of Dynamic Variations in Engine-Inlet Pressure on the Compressor System of a Twin-Spool Turbofan Engine, by J. E. McAulay, September 1970.

11. Brunda, D. F. and Boytos, J. F., A Steady-State Circumferential Inlet Pressure Distortion Index for Axial-Flow Compressors, paper presented at the ASME Gas Turbine Conference Products Show, Houston, Texas, March 28-April 1, 1971.

12. NASA TMX-1947, Performance and Stall Limits of an Afterburner Equipped Turbofan Engine With and Without Inlet Flow Distortion, by R. A. Werner, and others, April 1970.

13. Farmer, C. J., Inlet Distortion, Vorticity, and Stall in an Axial-Flow Compressor, M. S. Thesis, Naval Postgraduate School, Monterey, March 1972.

14. Povolny, J. H., and others, Effects of Engine Inlet Disturbances on Engine Stall Performance, paper presented at Aircraft Propulsion Conference, Cleveland, Ohio, 18-19 November 1970.

15. Gabriel, D. S., and others, Some Effects of Transients in Inlet Pressure and Temperature on Turbojet Engine, Preprint 709, LAS, New York, New York, January 1957.

16. NACA RM E57022, A Study of Temperature Transients at the Inlet of a Turbojet Engine, by L. E. Wallner, J. W. Useller and M. J. Saari, 1957.

17. NACA RM E55E25, Stall and Flame-Out Resulting from Firing of Armament, by J. H. Childs, and others, 1955.

18. AIAA Paper No. 70-625, The Effect of Inlet Temperature Distortion on the Performance of a Turbofan Engine Compressor System, by R. A. Rudey and R. J. Antl, 1970.

19. Tomassetti, N. R., Steam Ingestion by Aircraft Gas Turbine Engines, paper presented at National Conference on Environmental Effects on Aircraft and Propulsion Systems, 7th, Princeton, New Jersey, 25-27 September 1967.

20. Tomassetti, N. R. and Mink, G. R., Steam Ingestion by Aircraft Gas Turbine Engines-II, paper presented at National Conference on Environmental Effects on Aircraft and Propulsion Systems, 8th, Bordentown, New Jersey, 8-10 October 1968.

21. Mallett, W. E. and Parcells, E. M., Catapult Steam Ingestion Test of Three Turbofan Engines in the A-7 Aircraft, paper presented at the National Conference on Environmental Effects on Aircraft and Propulsion Systems, 10th, Trenton, New Jersey, 18-20 May 1971.

22. NAPTC-ATD-183, Steam Ingestion Tests of a Pratt and Whitney Aircraft TF30-P-8 Turbofan Engine, by P. Worobei, November 1971.

23. NAPTC-ATD-162, J52-P-6A Engine, Sea Level Missile Exhaust Gas Ingestion Tests, by W. A. Rich and R. A. Real, May 1969.

24. Rich, W. A., The Simulation of the Ingestion of Missile Exhaust by Turbojets, paper presented at the National Conference on Environmental Effects on Aircraft and Propulsion Systems, 10th, Trenton, New Jersey, 18-20 May 1971.

25. General Electric Report R71AEG32, TF34-GE-2 Engine Qualification, Rocket Gas Ingestion Test, by T. J. McCarey and J. A. Stephens, 31 December 1971.

26. Mokelke, H., The Unsteady Response of an Axial Flow Compressor with a Distorted Inlet Flow, paper submitted to the Turbomachinery Sub-Committee of the A. R. C. meeting, 2 October 1970.

27. Marble, F. E., "The Flow of a Perfect Fluid Through an Axial Turbomachine with Prescribed Blade Loading," Journal of the Aeronautical Sciences, v. 15, p. 473-485, August 1948.

28. Marble, F. E., "Three-Dimensional Flow in Turbomachines," Aerodynamics of Turbines and Compressors, edited by W. R. Hawthorne, p. 83-165, Princeton, 1964.

29. Carta, F. O., "Unsteady Normal Force on an Airfoil in a Periodically Stalled Inlet Flow," Journal of Aircraft, v. 4, p. 416-421, October 1967.

30. Dzung, L. S. and Seippel, C., "Aerodynamic Aspects of Blading Research," Flow Research on Blading, edited by L. S. Dzung, p. 1-50, Elsevier, 1970.

31. Air Force Systems Command, Foreign Technology Division Report AD 721 959, Unsteady Flow Around and Aeroelastic Vibration in Turbomachine Cascades, by G. S. Samoylovich, 23 February 1971.

32. Ericsson, L. E. and Reding, J. P., "Unsteady Airfoil Stall, Review and Extension," Journal of Aircraft, v. 8, p. 609-616, 1971.

33. AIAA Paper No. 70-131, Inviscid Flow through Cascades in Oscillatory and Distorted Flow, by B. Schorr and K. C. Reddy, January 1970.

34. Woods, J. R., Jr., The Analytical Treatment of Secondary Flows and Associated Losses in Axial-Flow Turbomachines, a paper prepared at the Naval Postgraduate School, Monterey, Calif., 10 December 1971.

35. Griepentrog, H., Prediction des Performances des Grilles d'Aubes Transsoniques a Hute Deflexion et Faible Allongement, Institut von Karmen Note Technique 59, December 1969.

36. Lakshminarayana, B. and Horlock, J. H., "Review: Secondary Flows and Losses In Cascades and Axial-Flow Turbomachines," International Journal of Mechanical Sciences, v. 5, p. 287-307, 1963.

37. Squire, H. B. and Winter, K. G., "The Secondary Flow in a Cascade of Airfoils in a Nonuniform -Stream," Journal of the Aeronautical Sciences, v. 18, p. 271-277, April 1951.

38. Hawthorne, W. R., "Rotational Flow Through Cascades, Part I. The Components of Vorticity," Quarterly Journal of Mechanics and Applied Mathematics, v. VIII, p. 266-279, 1955.

39. Private Communication, Richard A. Rudey, NASA Lewis Research Center, Cleveland, Ohio, 10 December 1971.

40. Private Communication, Richard A. Rudey, NASA Lewis Research Center, Cleveland, Ohio, 7 April 1972.

41. Hawthorne, W. R., "Secondary Circulation in Fluid Flow," Proceedings of the Royal Society, v. 206, p. 374-387, May 1951.

42. Hawthorne, W. R. and Novak, R. A., "The Aerodynamics of Turbomachinery," Annual Review of Fluid Mechanics, edited by W. R. Sears, p. 341-366, Annual Reviews, 1969.

43. Hawthorne, W. R., and Armstrong, W. D., "Rotational Flow through Cascades, Part II. The Circulation about the Cascade," Quarterly Journal of Mechanics and Applied Mathematics, v. VIII, p. 280-292, 1955.

44. Lakshminarayana, B., "Loss Evaluation Methods in Axial-Flow Compressors," Proceedings of the Workshop on Flow in Turbomachines, Naval Postgraduate School Report No. NPS-57VA1111A, edited by M. H. Vavra, K. D. Papilou, and J. R. Woods, Jr., 16 November 1971.

45. Liepmann, H. W. and Roshko, A., Elements of Gasdynamics, p. 191-193, Wiley, 1957.

46. NACA TN 2119, Effect of Humidity on Performance of Turbojet Engines, by J. C. Samuels and B. M. Gale, June 1950.

47. Tsien, H. S. and Beilock, M., "Heat Source in Uniform Flow," Journal of Aeronautical Science, v. 16, p. 756, 1949.

48. Rudinger, G., Wave Diagrams for Nonsteady Flow in Ducts, D. Van Nostrand, New York, 1955.

49. International Business Machines Corporation Form GH20-0205-4 System/360 Scientific Subroutine Package, Version III, Programer's Manual, p. 121-123, August 1970.

BIBLIOGRAPHY

1. AIAA Paper No. 68-58, Unsteady Aerodynamic and Stall Effects on Helicopter Rotor Blade Airfoil Sections, by J. Liiva, January 1968.

2. A.R.C. Report 17519, Some Formulae for the Calculation of Secondary Flow in Cascades, by W. R. Hawthorne, March 1955.

3. A.R.C. Reports and Memoranda No. 3483, Leakage and Secondary Flows in Compressor Cascades, by B. Lakshminarayana and J. H. Horlock, March 1955.

4. Crandall, S. H., Engineering Analysis, A Survey of Numerical Procedures, p. 243-246, McGraw-Hill, 1956.

5. Horlock, J. H., "Vorticity Transfer and Production in Steady Inviscid Flow," Journal of Basic Engineering, p. 65-70, March 1968.

6. Howell, A. R., "Flow in Cascades," Aerodynamics of Turbines and Compressors, edited by W. R. Hawthorne, p. 270-312, Princeton, 1964.

7. Kreyszig, E., Advanced Engineering Mathematics, Wiley, 1967.

8. Lakshminarayana, B. and Horlock, J. H., "Effect of Shear Flows on the Outlet Angle in Axial Compressor Cascades - Methods of Prediction and Correlation with Experiments," Journal of Basic Engineering, v. 89, p. 191-200, March 1967.

9. Preston, J. H., "A Simple Approach to the Theory of Secondary Flows," The Aeronautical Quarterly, v. V, p. 218-234, September 1954.

10. Rannie, W. D., "The Axial Compressor Stage," Aerodynamics of Turbines and Compressors, edited by W. R. Hawthorne, p. 313-367, Princeton, 1964.

11. Rauscher, M., Introduction to Aeronautical Dynamics, Wiley, 1953.

12. Schlichting, H. and Das, A., "On the Influence of Turbulence Level on the Aerodynamic Losses of Axial Turbomachines," Flow Research on Blading, edited by L. S. Dzung, p. 243-274, Brown, Boveri and Co. Limited, 1970.

13. Shames, I. H., Mechanics of Fluids, McGraw-Hill, 1962.

14. Tsien, H. S., "The Equations of Gas Dynamics," Fundamentals of Gas Dynamics, edited by H. W. Emmons, p. 27-63, Princeton, 1958.

15. Vavra, M. H., Aero-Thermodynamics and Flow in Turbomachines, Wiley, 1960.

16. Von Kármán, T. and Tsien, H., "Lifting-Line Theory for a Wing in Non-Uniform Flow," Quarterly of Applied Mathematics, v. III, p. 1-11, April 1945.

INITIAL DISTRIBUTION LIST

		No. Copies
1.	Defense Documentation Center Cameron Station Alexandria, Virginia 22314	2
2.	Library, Code 0212 Naval Postgraduate School Monterey, California 93940	2
3.	Chairman, Department of Aeronautics Naval Postgraduate School Monterey, California 93940	1
4.	Professor Allen E. Fuhs Department of Aeronautics Naval Postgraduate School Monterey, California 93940	10
5.	LCDR Michael M. Iverson, USN Box 27 Gonzales, California 93926	2
6.	Professor M. H. Vavra Department of Aeronautics Naval Postgraduate School Monterey, California 93940	1
7.	Professor M. F. Platzer Department of Aeronautics Naval Postgraduate School Monterey, California 93940	1
8.	RADM Carl O. Holmquist, USN Chief of Naval Research Office of Naval Research Arlington, Virginia 22218	1
9.	Captain William Sallada, USN Office of Naval Research Arlington, Virginia 22218	1
10.	Mr. Joe Boytos Naval Air Propulsion Test Center Trenton, New Jersey 08628	1
11.	Dr. Herbert Mueller Code 310A Naval Air Systems Command Washington, D.C. 20360	1

12. Mr. Irv Silver — 1
Code 03B
Naval Air Systems Command
Washington, D.C. 20360

13. Dr. Frank Tanczos — 1
Code 03
Naval Air Systems Command
Washington, D.C. 20360

14. Mr. Karl Guttman — 1
Code 330
Naval Air Systems Command
Washington, D.C. 20360

15. Mr. Robert Brown — 1
Code 536
Naval Air Systems Command
Washington, D.C. 20360

16. Dr. H. O. Johnson — 1
Code 330
Naval Air Systems Command
Washington, D.C. 20360

17. Mr. Mel Hartmann — 1
NASA Lewis Research Center
Cleveland, Ohio 44135

18. Dr. Ralph Roberts — 1
Office of Naval Research
800 North Quincy Street
Arlington, Virginia 22217

19. Mr. Eric Lister — 1
R. & T. Division
Naval Air Propulsion Test Center
Trenton, New Jersey 08628

20. Mr. Albert Martino — 1
R. & T. Division
Naval Air Propulsion Test Center
Trenton, New Jersey 08628

21. Mr. James Patton, Jr. — 1
Office of Naval Research
Arlington, Virginia 22218

22. Dr. Peter Crimi — 1
AVCO Systems Division
201 Lowell Street
Wilmington, Massachusetts 01887

23. M. l'Ingenieur en Chef Marc Pianko — 1
Service Technique Aeronautique
4 Avenue de la Porte d'Issy
75 Paris 15eme FRANCE

24. Mr. J. Surugue — 1
Directeur, Energie et Propulsion
ONERA
29 Avenue de la Division Leclerc
92 Chatellon-sous-Bagneux, FRANCE

25. Dr. M. Dunham — 1
National Gas Turbine Establishment
Pyestock
Farnborough Hants GREAT BRITAIN

26. Professor Kuhl — 1
D.V.L.
505 Porz Wahn
Linder Hohe
Allemagne GERMANY

27. Mr. Clifford Simpson — 1
AFAPL/TB
Wright-Patterson A.F.B., Ohio 45433

28. Professor Gordon Oates — 1
University of Washington
Seattle, Washington 98105

29. Professor Robert Goulard — 1
Director, Project SQUID
Purdue University
Lafayette, Indiana

30. Mr. J. F. Chevalier — 1
SNECMA
Centre d'Essais de Villaroche
77 Moissy-Cramayel FRANCE

31. Mr. M. Van Staveren — 1
Institute for Applied Research TNO
Post bus 406
Delft NETHERLANDS

32. Mr. Hill Barrett — 1
Detroit Diesel Allison
General Motors Corp.
Indianapolis, Indiana 46206

33. Professor Antonio Ferri — 1
Department of Aeronautics and Astronautics
School of Engineering and Science
New York University
Bronx, New York 10453

34. Mr. Elmer G. Johnson
Director, Fluid Dynamics Facilities
Research Laboratory
USAF Aerospace Research Laboratories
WPAFB, Ohio 45433 — 1

35. Mr. Marvin Stibich
Turbine Engine Division
AFAPL
WPAFB, Ohio 45433 — 1

36. Dr. A. A. Mikolajczak
Pratt and Whitney Aircraft
East Hartford, Connecticut 06108 — 1

37. Dr. Peter Trimm
Detroit Diesel Allison
General Motors Corp.
Indianapolis, Indiana 46206 — 1

38. Professor Duncan Rannie
California Institute of Technology
Pasadena, California 91109 — 1

39. Professor Jack Kerrebrock
Aeronautics and Astronautics
Massachusetts Institute of Technology
Cambridge, Massachusetts 02138 — 1

40. Professor George Serovy
Iowa State University
Ames, Iowa 50010 — 1

41. Professor Alan Stenning
Lehigh University
Bethlehem, Pennsylvania 18015 — 1

42. Dr. Gary R. Ludwig
Aerodynamics Research
Cornell Aeronautical Laboratory, Inc.
Buffalo, New York 14221 — 1

43. Mr. James E. Calogeras
NASA Lewis Research Center
Cleveland, Ohio 44135 — 1

44. Mr. F. E. Schubert
AFAPL/TB
Wright-Patterson AFB, Ohio 45433 — 1

45. Dr. Gunnar Broman
Vice President, Engineering
VOLVO Flygmotor
Trollhattan, SWEDEN — 1

46. Mr. Robert Zalis
MZ 240 GF
1000 Western Avenue
Lynn, Massachusetts 01910 — 1

47. Mr. Paul H. Kutschenreuter, Jr.
Mail Drop E 198
General Electric Company
Cincinnati, Ohio 45215 — 1

48. Mr. David Jamison
General Electric Company
P.O. Box 2143
Kettering Branch
Dayton, Ohio 45429 — 1

49. Prof. Jacques Valensi
Director Institut de Mecanique des Fluides
l'University d'Aix-Marseille
Marseille, FRANCE — 1

50. Professor Jacques Chauvin
Von Karman Institute for Fluid Mechanics
72 Chaussee de Waterloo
1640 Rhode-St-Genese BELGIUM — 1

51. Mr. Marvin F. Schmidt
Turbine Engine Division
AFAPL
WPAFB, Ohio 45433 — 1

52. Mr. J. W. McBride
General Electric Company
Evandale, Ohio 45215 — 1

53. Dr. Leroy H. Smith, Jr.
General Electric Company
Evandale, Ohio 45215 — 1

54. Professor B. Lakshminarayana
Pennsylvania State University
State College, Pennsylvania — 1

55. Professor Jean Louis
MIT Gas Turbine Laboratory
Massachusetts Institute of Technology
Cambridge, Massachusetts 02138 — 1

56. Dr. F. O. Carta
United Aircraft Research Labs.
United Aircraft Corporation
400 Main Street
East Hartford, Connecticut 06108 — 1

57. Mr. Norman Cotter 1
Pratt and Whitney Florida Research Center
West Palm Beach, Florida 33402

58. Dr. George L. Mellor 1
Princeton University
Forrestal Campus
Princeton, New Jersey 08540

59. Mr. Stan Ellis 1
Pratt and Whitney Florida Research Center
West Palm Beach, Florida 33402

60. Mr. David Bowditch 1
NASA Lewis Research Center
Cleveland, Ohio 44135

61. Professor Frank Marble 1
California Institute of Technology
Pasadena, California 91109

62. Dr. W. Z. Sadeh 1
Engineering Research Center
Colorado State University
Ft. Collins, Colorado 80521

63. Professor Bruce A. Reese 1
School of Mechanical Engineering
Purdue University
Lafayette, Indiana 47907

64. Professor P. C. Adamson, Jr. 1
Department of Aerospace Engineering
University of Michigan
Ann Arbor, Michigan 48103

65. Professor W. R. Sears 1
Grumman Hall
Cornell University
Ithaca, New York 14850

66. Professor J. E. McCune 1
M.I.T. - 37 - 391
Cambridge, Massachusetts 02139

67. Dr. Jack Nielsen 1
Nielsen Engineering and Research, Inc.
850 Maude Avenue
Mountain View, California 94040

68. John Scott 1
School of Engineering and Applied Science
University of Virginia
Charlottesville, Virginia 22901

69. W. F. O'Brien 1
Mechanical Engineering Department
Virginia Polytechnic Institute and State University
Blacksburg, Virginia 24061

70. Dr. W. Heiser 1
AFAPL
WPAFB, Ohio 45433

71. J. P. Johnston 1
Mechanical Engineering Department
Stanford University
Stanford, California

72. John Povolny 1
NASA Lewis Research Center
Cleveland, Ohio 44135

73. Lt. Clinton J. Farmer 1
18573 Antelope Drive
Lemoore, California 93245

74. Richard A. Rudey 1
NASA Lewis Research Center
Cleveland, Ohio 44135

Security Classification

DOCUMENT CONTROL DATA - R & D

(Security classification of title, body of abstract and indexing annotation must be entered when the overall report is classified)

1. ORIGINATING ACTIVITY *(Corporate author)*

Naval Postgraduate School
Monterey, California 93940

2a. REPORT SECURITY CLASSIFICATION

Unclassified

2b. GROUP

3. REPORT TITLE

Conversion of Inlet Temperature Distortions to Vorticity for an Axial-Flow Compressor

4. DESCRIPTIVE NOTES *(Type of report and, inclusive dates)*

Master's Thesis; June 1972

5. AUTHOR(S) *(First name, middle initial, last name)*

Michael Martin Iverson

6. REPORT DATE	7a. TOTAL NO. OF PAGES	7b. NO. OF REFS
June 1972	98	49

8a. CONTRACT OR GRANT NO.	9a. ORIGINATOR'S REPORT NUMBER(S)
b. PROJECT NO.	
c.	9b. OTHER REPORT NO(S) *(Any other numbers that may be assigned this report)*
d.	

10. DISTRIBUTION STATEMENT

Approved for public release; distribution unlimited.

11. SUPPLEMENTARY NOTES	12. SPONSORING MILITARY ACTIVITY
	Naval Postgraduate School Monterey, California 93940

13. ABSTRACT

A survey of the literature on pressure, temperature and foreign gas inlet distortions is made. For interpretation of the influence of inlet distortion on engine stability, a break is made with distortion methods which use temperature or pressure distortion maps. The distortion in the form of temperature contours is transformed to vorticity using appropriate equations derived for both incompressible and compressible flow. Crocco's theorem has been expanded in scope to include multispecie, nonuniform, perfect gas mixtures. The derivation of the equations and specialization to cases of interest involved a thorough order of magnitude analysis. A numerical solution of Poisson's equation as formulated by Squire and Winter to describe secondary flow arising from convected vorticity is presented. Deficient areas of knowledge relating to the general temperature/foreign gas problem are outlined. A conceptual model involving compressor stage transfer functions and feedback mechanisms is introduced and discussed at several points. Although not essential to understanding the vorticity-stall logic chain, this model is a useful conceptual tool and may be worthy of additional study.

DD FORM 1 NOV 65 1473 (PAGE 1)

S/N 0101-807-6811

Security Classification

A-31408

14. KEY WORDS	LINK A		LINK B		LINK C	
	ROLE	WT	ROLE	WT	ROLE	WT
Compressor Stall						
Aircraft Inlet/Temperature Distortion						
Aircraft Gas Turbines						
Compressor Inlet Temperature Distortion						
Steam Ingestion						
Missile Exhaust Gas Ingestion						
Rocket Exhaust Gas Ingestion						